PHILOSOPHICAL TRANSACTIONS OF THE ROYAL SOCIETY A MATHEMATICAL, PHYSICAL & ENGINEERING SCIENCES

Stored Energy in the Graphite of Power-Producing Reactors

J. C. Bell, H. Bridge, A. H. Cottrell, G. B. Greenough, W. N. Reynolds and J. H. W. Simmons

Phil. Trans. R. Soc. Lond. A 1962 **254**, 361-395
doi: 10.1098/rsta.1962.0002

STORED ENERGY IN THE GRAPHITE OF POWER-PRODUCING REACTORS

By J. C. BELL,* H. BRIDGE,† A. H. COTTRELL, F.R.S.,‡ G. B. GREENOUGH,§ W. N. REYNOLDS|| and J. H. W. SIMMONS||

(*Received* 26 *July* 1961)

CONTENTS

The effects of the atomic displacements produced in graphite by the collisions of fast neutrons are of great importance in the technology of graphite-moderated nuclear power reactors. This paper describes experimental and theoretical work on the stored energy associated with such displacements, the rate of release of this stored energy as a function of temperature, and the thermal conductivity of graphite, over a range of irradiation and annealing conditions.

Some large effects are observed, particularly in the rate of accumulation of radiation damage at various temperatures of irradiation, as well as many other effects of fundamental interest. After high doses at low irradiation temperatures the rate of release of stored energy with increasing temperature can approach the specific heat of unirradiated graphite, but a relatively small increase in the irradiation temperature brings about a drastic reduction in the amount of energy stored.

The conditions under which this radiation damage is produced are very complicated, for they involve not only sequences of spontaneous rearrangements amongst the displaced atoms during and after the irradiation treatment but also the total intensity and the energy spectrum of the neutrons, and it is impossible to separate all the variables in a strict sense. Various experiments have however been made, and theoretical and semi-empirical procedures developed, which enable results to be correlated satisfactorily over a range of conditions including those in both graphite-moderated and water-moderated reactors. The paper shows how the rate of stored energy release may be estimated for practical values of temperature and irradiation dose.

* Formerly at *Research and Development Laboratories, Windscale*; now at *Lucas Heights, Australia*.

† Formerly at *Research and Development Laboratories, Windscale*; now at *Reactor Material Laboratories, Culcheth*.

‡ Formerly at *Atomic Energy Research Establishment, Harwell*; now at *Department of Metallurgy, University of Cambridge*.

§ Formerly at *Research and Development Laboratories, Windscale*; now at *Reactor Fuel Laboratories, Springfields*.

|| *Atomic Energy Research Establishment, Harwell*.

1. Introduction

When a fast neutron collides with a carbon nucleus, while passing through graphite in a nuclear reactor, about 100 nearby atoms are knocked out of lattice positions and injected into the immediately surrounding material. In this way a prolonged neutron irradiation (e.g. 10^{20} n cm^{-2}) at ambient temperature displaces about 1 to 3% of all atoms in the material. Basically, two simple types of lattice point defects, *interstitials* which are the displaced atoms themselves and *vacancies* which are the atomic holes left behind, are produced in equal numbers. In practice, however, the 'damage' is more complicated than this because these point defects are created as, or quickly regroup themselves into, clusters of various sizes and forms with a wide range of physical behaviour.

This radiation damage alters many properties of the material, including properties important to the functioning of graphite-moderated reactors (Simmons 1960; Nightingale, Davidson & Snyder 1958). One of these is the stored energy. Some 5 to 10 eV per displacement is associated with the broken atomic bonds and lattice strains round the defects. In heavily irradiated graphite this stored energy, which can amount to as much as 600 cal g^{-1} (Woods, Bupp & Fletcher 1956) is sufficiently large in relation to the specific heat of the material, which ranges from 0·2 cal g^{-1} degC^{-1} at room temperature to 0·45 cal g^{-1} degC^{-1} at 700 °C, to raise the temperature of the material by several hundred degrees if suddenly released as heat. Such energy releases can in fact occur because the lattice defects, particularly the interstitials, can move about inside the crystals with the help of thermal activation and so take part in various annealing processes in which the clusters rearrange themselves into more stable forms, or in which migrating defects disappear when they meet defects of opposite type or meet free surfaces, intercrystalline boundaries, and dislocations.

Because the defects form clusters of various stabilities and mobilities the annealing of irradiated graphite consists of a complex sequence of processes, the details of which remain largely unravelled. Some general principles are clear, however. The lifetimes of the various defects, before annihilation or regrouping, are spread widely over a time scale that becomes progressively shorter at higher temperatures, so that at any temperature some annealing is possible, i.e of those defects whose lifetimes compare with the annealing time.

Superposed on this general background of behaviour are two additional features. First, large annealing 'peaks' appear at those temperatures where particularly abundant species of defects become mobile. In graphite irradiated at ambient temperature one such peak appears in the range 100 to 200 °C and the amount of energy released in it is sufficient, in heavily irradiated material, to raise the temperature rapidly (e.g. within 10^3 s) and spontaneously to 300 to 500 °C (Bell & Greenough 1957). To avoid adventitious, self-sustaining, energy releases of this kind in air-cooled graphite-moderated reactors it has become general practice to induce smaller releases deliberately in a controlled manner at suitable intervals during the life of the reactor (Command 471, 1958).

A study of the reaction kinetics and other aspects of self-sustaining releases in air-cooled reactors has been described elsewhere (Lomer 1957; Cottrell, Lomer, Simmons,

Bell & Greenough 1958) and will not be further discussed here. The purpose of the work described below was to determine the stored energy of graphite under conditions expected in power-producing reactors. This knowledge was needed to decide certain aspects of the design and operation of such reactors; for example, whether it was necessary to raise the temperature of the graphite moderator (by raising the inlet temperature or by shielding the graphite from the coolant) so as to reduce the rate of energy storage; or whether arrangements should be made to enable such reactors to be annealed periodically either by means of self-sustaining releases or by running for a limited time at low power and high temperature. Above all, it was necessary to ascertain the rates of energy release in the graphite moderator at temperatures in the range 150 to 650 °C. This rate is most conveniently measured as the temperature coefficient, $\mathrm{d}E/\mathrm{d}T$, of release of energy E at a standard rate of heating (e.g. 2 degC min^{-1}) because $\mathrm{d}E/\mathrm{d}T$ is dimensionally comparable with the specific heat c of the material. This provides a basis for deciding the safe operation of a reactor as regards release of stored energy. Although the precise choice of the maximum permissible $\mathrm{d}E/\mathrm{d}T$ depends on a detailed analysis of general reactor behaviour that lies beyond the scope of this paper, it is clear that provided $\mathrm{d}E/\mathrm{d}T$ is appreciably smaller than (e.g. 80% of) c at the rates of heating which might be encountered in practice, the effective specific heat of the graphite will remain positive and self-sustaining releases cannot occur.

Previous experimental work on the graphite of air-cooled reactors, although enlightening, was of little quantitative value in this problem because the graphite in a power-producing reactor is irradiated at a higher rate (e.g. 10^{13} n $\mathrm{cm}^{-2}\,\mathrm{s}^{-1}$), to a much higher dose (e.g. 10^{22} n cm^{-2}), and at a higher temperature (e.g. 150 to 350 °C). The first two of these increase the amount of energy stored but the third decreases it, so that the net effect is uncertain. Moreover, the important types of defects in the two cases are almost certainly different, so that low-dose low-temperature irradiations provide no guide to the behaviour of graphite under high-dose, high-temperature, conditions. For example, the power reactor temperatures lie within or above the range of the 100 to 200 °C annealing peak, so that the particular defects responsible for this peak cannot accumulate in important amounts; on the other hand, because the neutron dose is so much higher, there is no *a priori* reason why other types of defects, unimportant in the low-dose low-temperature graphite, should not accumulate in amounts sufficient to give self-sustaining releases.

It was therefore necessary to investigate experimentally the accumulation of stored energy in graphite under these new conditions. The main problem was one of time; to produce, under well-controlled conditions, graphite very heavily irradiated at the appropriate temperatures in sufficient time to help the reactor designs. An extensive series of monitor samples of graphite placed in the first Calder Hall reactors has provided and still provides a means of keeping directly in touch with the progress of stored energy in power-reactor moderators. For design purposes, however, it was necessary to provide, in a 2-year experiment, an irradiation dose equal to that obtained over 20 years in a power reactor. The only way to achieve this was to make use of the much higher neutron fluxes (e.g. up to 5×10^{13} n $\mathrm{cm}^{-2}\,\mathrm{s}^{-1}$) available in certain positions in heavy-water-moderated testing reactors. To obtain the highest possible fast neutron flux it was decided to irradiate samples in the interior of specially designed hollow fuel elements fitted into the central

region of the DIDO reactor at Harwell (or in PLUTO at Harwell or in DMTR at Dounreay). Most of the results described below were obtained in this way.

The acceleration of the rate of irradiation and the use, for the experimental programme, of a reactor the neutron energy spectrum of which differs from that of graphite moderated reactors, produced two major difficulties of interconverting the results. These had to be overcome before the prime technical purpose of the work could be accomplished, and an appreciable part of this paper is devoted to an examination of this problem.

The effect of rate of irradiation results from the balance between the production of damage by radiation and its annealing by thermal activation, processes which occur concurrently at the temperatures of power-producing reactors. An increase in the rate of irradiation is therefore approximately equivalent to a decrease in the temperature of irradiation and, if the annealing kinetics are known, it it possible to allow for its effect in terms of an 'equivalent temperature'. The standard rate of irradiation is defined, arbitrarily, as the rate of irradiation at the wall of a fuel channel in Calder where the rate of energy production by fission in the neighbouring uranium is 3·12 MW/a.t* The Calder equivalent temperature is the basis of comparison of results.

The effect of the neutron energy spectrum results from the fact that a fast neutron is capable of displacing more atoms than a slow one. Since neutrons are moderated in passing from the surface of a fuel element to the centre of a graphite block, or in passing through heavy water, the rate of accumulation of damage varies from the surface to the interior of the blocks in a graphite moderator, and with the position of experimental samples in a testing reactor. Even more important is the difference between the two types of reactor. There are no generally satisfactory methods of establishing neutron energy spectra in reactors, nor is there exact knowledge of the damage produced by neutrons of different energies. Recourse was therefore made to empirical methods of correlation. Fortunately it appeared that the activity produced in nickel by an (n, p) reaction with a threshold of about 3 MeV, was related to the rate of production of irradiation damage in graphite by a factor which did not vary greatly from one position to another. An arbitrary unit of dose is necessary and in this case the Calder equivalent dose is used, i.e. the damage dose received by the graphite at the wall of a fuel channel when the uranium in the neighbourhood had produced 1 MW/a.t of energy for 1 day, 1 MWd/a.t.

2. Experimental details

(*a*) *Irradiation techniques*

There are two main methods of carrying out irradiation experiments: in the first, the experimental conditions are broadly defined by the ambient reactor conditions, while in the second an experimental assembly, the 'rig', is designed to maintain the desired conditions despite variations in the reactor conditions. In experiments carried out under ambient conditions there is usually ample space with little restriction on specimen size. In this type of experiment the choice of conditions is limited because the irradiation

* The standard unit of rate of energy production by fission is megawatts per tonne of fuel. Since the damage to the graphite at the wall of a fuel channel is mainly determined by the fission of uranium in the immediate vicinity, the standard chosen for the rate of irradiation is megawatts in the adjacent fuel elements per tonne of fuel, abbreviated to MW/a.t, the a. standing for *adjacent* and t for *tonne*.

temperature is related to the neutron flux. Furthermore, temperature variations occur owing to variations in the local flux level. It is usually necessary to use ambient conditions in production reactors. In these reactors access to specimens for temperature measurement and examination is restricted and the rate of accumulation of neutron dose is relatively low.

In the present work it was essential to undertake experiments in the material-testing reactors to provide data as rapidly as possible, and in the Calder Hall reactors to provide results relevant to the appropriate power reactor conditions of flux spectrum and intensity, for the purpose of comparison. High flux experiments in the material-testing reactors were undertaken in a new type of rig, designed for this purpose, while those in the Calder Hall reactors were restricted by operational requirements to ambient conditions.

A major difficulty in a rig in a high flux reactor is that of precise temperature measurement and control due to the high rate of heat generation caused by neutron and γ-ray absorption in both specimens and rig parts. Consider, for instance, a graphite specimen irradiated in a fast neutron flux of 3×10^{13} cm^{-2} s^{-1} at a temperature of 200 °C, where the average temperature is required to within 5 degC and temperature gradients in the specimen are to be limited to a similar value. Nuclear heating in graphite under these conditions is of the order of 2 W g^{-1} and the thermal conductivity after some irradiation 1×10^{-2} cal cm^{-1} s^{-1} degC^{-1}. This would give a difference of temperature of 5 degC in a 1 cm cylinder in a uniform temperature enclosure; uniform heat transfer to the enclosure must also be ensured. There are also difficulties because the dimensions and thermal conductivity of the specimen change during the period of irradiation. Also it is difficult under such conditions to maintain a contact between a specimen and an attached thermocouple sufficient to guarantee an accurate value of the measured specimen temperature, without radically altering the temperature distribution in the specimen or subjecting the graphite to stress during the experiment.

(i) *Experiments in Calder Hall reactors*

The Calder Hall reactors (Moore & Goodlet 1957) are of the graphite-moderated type, using natural uranium fuel and carbon dioxide coolant, with a core 32 ft. in diameter and 26 ft. high. Fuel channels, varying in diameter between 4·1 and 3·61 in. according to position, are arranged vertically on an 8 in. square lattice, access to each group of 16 channels being made through an overhead entry port in the steel pressure vessel and the biological shield. A diagram of the graphite lattice is shown in figure 7. At the centre of each group of fuel channels is situated an additional channel, termed the 'x-hole', normally 3·25 in. in diameter although one often used was 4·0 in. diameter.

Measurements were made on specimens irradiated in containers loaded into the x-holes and on specimens machined from the walls of selected fuel channels. x-hole specimens were mounted in graphite holders in graphite or Magnox containers. Fifteen containers completed the loading for each channel and each held sixteen specimens allocated to stored energy determinations; the coolant had limited access to the specimens by diffusion through the graphite holders.

Direct measurement of specimen temperatures was difficult owing to the need to pass the connecting leads through the pressure vessel and to the handling problems

associated with the highly radioactive thermocouple materials. It was originally proposed to restrict coolant flow in these channels and to estimate the specimen temperatures from the temperature of the adjacent moderator, as measured by thermocouples built into the reactor during the original construction. Early comparative measurements of property changes showed this method to be grossly in error, mainly because of the leakage of gas into the central channel from the surrounding fuel channels. Two investigations were undertaken. In the first a relaxation calculation was carried out on a Mercury computer which took into account variations in gas flow in the central channel and adjacent fuel channels, interchannel gas leakage, profile of the container, nuclear heating in the specimen assemblies and the surrounding moderator, and radiation and conductive heat transfer. Results for a typical channel are shown in figure 1 (A. Nicklin, private communication).

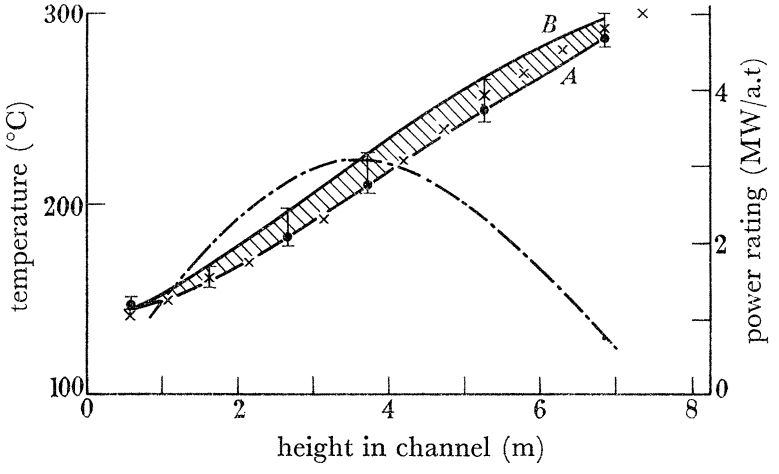

FIGURE 1. Calder Hall reactors: experimental channel specimen temperatures and adjacent fuel element power ratings. ———, Measured specimen temperature (*A* and *B*: average temperatures at start and end of 135 day cycle, respectively); ⊕, limits of temperature transients; ×, calculated temperatures; –·–·–·–·–, fuel element power rating.

At a later date special equipment for measuring temperatures was loaded into a normal and a wide diameter experimental channel. Both specimen and container temperatures were measured. Special shielded plugs carried the electrical leads through the reactor vessel and the assemblies were removed in shielded flasks, some 30 ft. in height, at the end of the experiment. Results for an experimental channel are summarized in figure 1. Temperature variations and fluctuations could be correlated with variations in the reactor flux distribution and power: the average specimen temperatures increased over a period of about 135 days and then returned to their original values. The extent of the variation depended on the position in the channel and is shown as a shaded band in figure 1. In addition, temperature transients covering periods of up to a few hours were also detected: the maximum deviations from the average temperatures are indicated in figure 1.

Temperatures in the moderator were more stable than in the experimental channels and it was decided to cut specimens direct from the inner walls of a few central fuel channels. In its final form the 'coring' machine consisted of a cylindrical shell which was lowered into a channel and clamped at a predetermined position after the reactor had been cooled.

A small pneumatically driven turret equipped with diamond-tipped cutting arms bored into the channel wall and isolated a small graphite core. At the end of the radial travel of the turret, the arms pivoted and severed the core completely from the block; the turret containing the sample then retracted into the shell and the machine was extracted. During these operations the cutting head and the sample were cooled in an air stream to minimize the risk of an excessive temperature rise with the associated thermal annealing of the irradiation damage. Samples obtained in this way were approximately $\frac{5}{8}$ in. diameter and 1 in. long.

Radiation exposures for the various sample positions were derived from the time integrals of the reactor flux distributions as determined from the relative flux distributions (measured in terms of the activity of irradiated tungsten wire) and the reactor heat outputs. A flux distribution, expressed in terms of the heat rating of the fuel, is given in figure 1 for a typical fuel channel: the equivalent ratings for an experimental channel may be obtained using the factors discussed in §3. Exposures obtained in this manner do not take fully into account local variations which may occur and are only accurate to about $\pm 10\%$.

The estimated fluxes were supplemented by direct measurements of thermal and fast fluxes, as measured by the activity of cobalt and nickel foils, at a limited number of sites. Characteristic values are given in table 1.

TABLE 1. CHARACTERISTICS OF CALDER HALL AND M.T.R. IRRADIATION FACILITIES

facility	type	ϕ_{Ni}(n cm^{-2}s^{-1})	practical exposure per year (MWd/a.t)
Calder experimental channel	ambient 150 to 280 °C	1×10^{12} (max.)	700 (max.)
test reactor hollow fuel element	controlled temperature	4×10^{13}	5000 to 6000

(ii) *Experiments in material-testing reactors*

The material-testing reactors DIDO and PLUTO (see, for example, *Nuclear Engineering* 1957) operate at a total heat rating of 10 MW using enriched uranium fuel with heavy water acting as both the moderator and the coolant. The core of this type of reactor consists of 25 box-type elements each containing 10 fuel plates and occupies a volume of 34 in. by 28 in. by 24 in. The irradiation sites originally provided in these reactors were situated in the moderator adjacent to the core and while these provided exceptionally high thermal flux levels, the fast fluxes available were too small to meet the requirements of the graphite irradiation programme. It was necessary to replace some of the standard fuel elements by a special type of element, in which the fuel plates were contained between two concentric tubes so as to provide an internal space for the specimens separated from the fuel by the minimum thickness of moderator. Characteristics of these hollow fuel elements are given in table 1.

The design of the rig is shown schematically in figure 2.

The outer container was a sealed thimble of Zircaloy or stainless steel (A) located along the axis of the hollow fuel element (B). Over the length of the thimble adjacent to the fuel approximately 2 ft. 5 in., the inner surface was honed to a diameter of $2{\cdot}008 \pm 0{\cdot}002$ in. with a maximum ovality of 0·0005 in. Individual rigs were matched with the appropriate

thimbles before assembly. Each thimble was maintained at a steady temperature by cooling with heavy water (I) at a mean temperature of 41 °C. Three specimen magazines (C) in the form of hollow cylinders of aluminium were suspended along the axis of a thimble each holding up to nine cylindrical graphite specimens (D) nominally 0·25 in. in diameter and up to 3 in. long, in holes parallel to the axis of the cylinder, and two flux monitors (E).

The gas gaps (F) between the magazine and the thimble were chosen to give approximately the required temperatures, fine control being obtained by adjusting the current in the heaters (G). For operation in helium the heat dissipated in a magazine was about

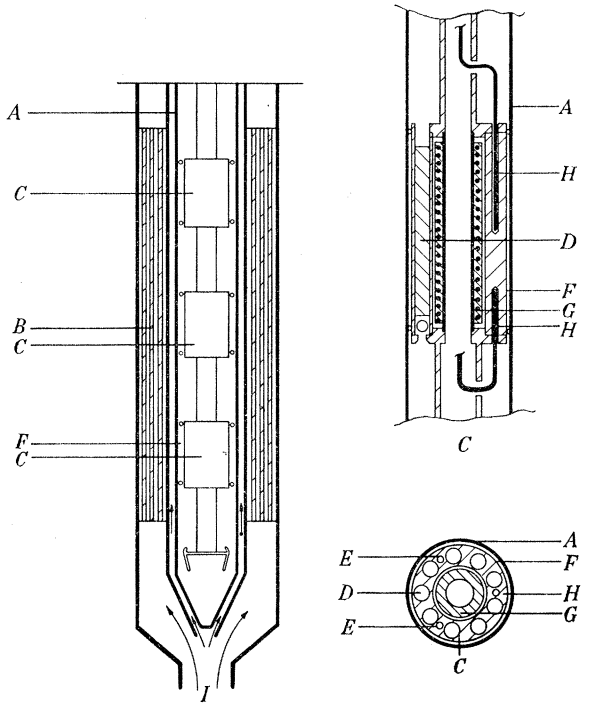

FIGURE 2. Material-testing reactor: hollow fuel element irradiation facility.

800 W and the corresponding gaps, measured at 20 °C, varied from 0·0065 in. for operation at 150 °C, to 0·025 in. for operation at 350 °C. These gaps were chosen to give a ratio of nuclear to electrical heating of 0·8, this being the optimum value for reducing gradients in the magazine while still retaining a sufficient margin of temperature control. The gaps between the specimens and the magazine were set initially at between 0·001 and 0·003 in.

The coaxial heaters fitted to each magazine consisted of 21 turns of 21 s.w.g. Bacrom wire set in ceramic cement (C 60 impregnated with sodium silicate and made up with demineralized water). Heater leads were of mineral-filled stainless-steel covered Pyrotenax cable with double Mangonic cores, a mechanical connexion being made to the heater winding.

Three stainless-steel sheathed, Chromel/Alumel thermocouples (H) were set into each magazine on the specimen radius: the top thermocouple was used to control the magazine temperature, while the middle and lower thermocouples actuated high- and low-temperature warning circuits (+5 and −7 degC, respectively) and automatic reactor shut-down circuits. Each magazine heater was controlled independently by a recorder-controller feeding a magnetic amplifier.

During operation the rig and thimble were filled with pure dry helium at a pressure of 15 Lb./in.^{2}; if a high impurity level was detected during the experiment purging and refilling could be carried out under power. Alarms were also fitted to warn against variations in the helium pressure or the influx of heavy water into the thimble.

Under normal operating conditions, the estimated average specimen temperature was 5 degC above the magazine temperature (Nicklin, private communication). The temperature gradient in a specimen was a function of the thermal conductivity of the specimen and of the ratio of nuclear to electrical heating: calculations showed that the extremities of an unirradiated 3 in. specimen could deviate by ± 6 degC from the temperature of the mid-point. For reductions in the thermal conductivity of the specimen by factors of 25 and 50, the extremities of the central $\frac{3}{4}$ in. section of the specimen could deviate by ± 5 and ± 10 degC respectively from the central temperature. Strict operating conditions for the rigs were enforced to ensure that temperatures did not deviate significantly from the nominal values. If the indicated temperature increased above the specified value the reactor was shut-down and the rig removed for examination, specimens subjected to any rise greater than 10 degC usually being rejected. Similarly the maximum time that a rig could operate below temperature was restricted to ensure that no excessive error was introduced. Specimens were rejected if the total time spent at 5 degC below the set value exceeded 60 h in any period of 1000 h.

Specimens were removed for examination by withdrawing the central assembly into a vertical, shielded flask and transferring it to a viewing cell. This cell was a box some 4 ft. square and 2 ft. 6 in. in height with lead walls 6 in. thick, three adjacent walls being fitted with lead glass windows and bearings for remote handling tools. The magazine was positioned and the required specimen lifted, by inserting a pin through the base of the magazine, and transferred to a small transport flask.

The most serious practical difficulties encountered during operation of the experimental rigs were caused by mechanical failures of the electrical leads to the heaters and thermocouples; in the beginning such failures frequently ruined a rig after only a few weeks irradiation. The impossibility of simulating operating conditions in the laboratory made it necessary to test modifications to the design in the reactor and subsequently dismantle the rig with remote handling equipment to diagnose the cause of failure.

In the early designs of rig, heater leads were of copper insulated by alumina sleeves, the connexion to the heater being made by brazing or welding. Failure usually occurred at or near the joint because of embrittlement, resulting from the attack of copper oxide by residual hydrogen in the rig atmosphere, a reaction which was accelerated in the presence of radiation. Subsequent improvements were based on the use of oxygen-free copper, a reduction in the temperature of operation of the leads, and better mechanical support of the leads adjacent to the junction with the heater. Later, the use of Pyrotenax cables with nickel cores solved many of the problems although sulphur embrittlement of the nickel necessitated the complete elimination of rubber components and other sources of this impurity. Similar problems of thermocouple failures were finally solved by the use of Chromel-Alumel Pyrotenax cables.

The later designs of rig were very reliable and mostly operated successfully for periods of six months or more, during which time they were unloaded from the reactor several times.

PHILOSOPHICAL TRANSACTIONS OF THE ROYAL SOCIETY A MATHEMATICAL, PHYSICAL & ENGINEERING SCIENCES

(*b*) *Specimens and flux monitors*

All specimens examined were machined from British, reactor-grade, graphite blocks selected from current supplies denoted grade *A* (O'Driscoll & Bell 1960).

Specimens for irradiation in the Calder Hall reactors were $0{\cdot}5 \pm 0{\cdot}005$ in. o.d. and 2·0 in. in length, while those for irradiation in the M.T.R. rigs were $0{\cdot}248 \pm 0{\cdot}001$ in. o.d. and either 3·00 or 1·25 in. in length. Rig specimens were periodically passed through a standard die to retain the dimensional tolerances, thus reducing changes in heat transfer conditions and the risk of specimens sticking in the rig due to irradiation growth.

Reactor fluxes were measured by the ^{59}Co (n, γ) ^{60}Co and the ^{58}Ni (n, p) ^{58}Co reactions, conversions from activities to ϕ_{Co} and ϕ_{Ni} being made using the cross-sections given in table 2. In the rigs the monitors were in the form of thin wires contained in aluminium capsules approximately 0·5 in. in length, but in the Calder Hall reactors it was necessary to contain the foils in double stainless-steel capsules, which required additional calibration to allow for absorption in the stainless steel.

Certain specimens were machined after irradiation; to avoid thermal annealing the specimens were cooled during cutting.

TABLE 2. NUCLEAR DATA FOR FLUX MONITORS

reaction	cross-section (barns)	half-life
^{59}Co (n, γ) ^{60}Co	38·0	5·27 years
^{58}Ni (n, p) ^{58}Co	0·107	71·5 days

(*c*) *Methods of measurement*

The two major quantities in stored energy determinations are the rate of release of energy, in terms of time and annealing temperature, and the total quantity of energy stored. The latter may be measured directly by comparing the heats of combustion of irradiated and unirradiated material, the only limitation being the accuracy of the experimental method. However, measurements of the former are more complex and require consideration of the conditions under which the release takes place.

Various theoretical models representing the annealing of radiation-induced defects have been discussed in the literature (Lomer 1957; Nightingale & Fletcher 1957; Cottrell *et al.* 1958; Simmons 1960); the equations used were of the form:

$$\mathrm{d}E(t)/\mathrm{d}t = -F(E)\exp(-Q/kT), \tag{1}$$

where E is the energy remaining at time t, F is a function characterizing the state of the graphite, T is the absolute temperature, Q is an activation energy, and k is Boltzman's constant. The rate of change of specimen temperature is determined by

$$c(T)\,\mathrm{d}T/\mathrm{d}t = -\mathrm{d}E/\mathrm{d}t + h(T, t), \tag{2}$$

where $c(T)$ is the specific heat of the sample and $h(T, t)$ the heat lost or gained.

The specification of $h(T, t)$ determines the type of experiment undertaken. Conditions are usually chosen to correspond to some simple practical case in a reactor, e.g. adiabatic conditions, $h(T, t) = 0$, or a controlled rate of temperature rise. The quantity considered here is the energy released in unit temperature interval, $\mathrm{d}E/\mathrm{d}T$, when the temperature rises linearly with time.

Two types of calorimeter were used to measure dE/dT: the 'linear-rise calorimeter' and the 'modified adiabatic-rise calorimeter'. In the first, the temperature difference between the specimen and the calorimeter is kept at zero and the necessary heat is supplied directly to the specimen; in the second, the temperature difference is controlled in such a way as to maintain the linear rate of rise of specimen temperature.

(i) *The linear-rise calorimeter*

The initial form of this apparatus, designed for operation up to 500 °C at a linear rate of rise of temperature of 2 degC min^{-1}, has been described by Henson & Mounsey (1961), while a modified design for operation up to 750 °C at a rate of rise of 4 degC min^{-1} was described by Davidson, Harrison, Mounsey & Jacques (1961). The basic principle of operation was the same for both instruments: two specimens, one irradiated, the other an unirradiated standard, were mounted side by side in an enclosed, evacuated, copper calorimeter, the temperature of which rose linearly with time. Their temperatures were held equal to that of the calorimeter by two small internal heaters; for identical samples, the difference between the powers supplied to the heaters was a direct measure of the rate of energy release in the irradiated sample. Lack of symmetry between samples was allowed for from observations made during a second run, while incomplete annealing of the active sample during the first run could be detected from a third set of measurements (this correction was negligible except for a range of about 60 degC below the highest temperature reached in the first anneal).

A minimum specimen size of 1 in. by 0·5 in. o.d. was used in the 500 °C apparatus and one 2 in. by 0·5 in. o.d. in the 750 °C instrument. The estimated accuracy of each calorimeter was $\pm 0{\cdot}01$ cal g^{-1} $degC^{-1}$ ($\pm 2\sigma$), a value confirmed by the observed reproducibility of measurements on samples cut from a single irradiated specimen. Tests of the absolute calibration of the instrument, in which specimens of various masses and dimensions were used indicated a similar degree of precision.

(ii) *The modified adiabatic-rise calorimeter*

In its original form (Henson & Simmons 1959), the calorimeter was designed to investigate annealing of samples under adiabatic conditions. A small specimen was suspended within a copper calorimeter surrounded by radiation shields and enclosed in a water-cooled vacuum jacket. The release of energy was started by supplying a known amount of heat to the specimen cavity and the calorimeter temperature was then maintained equal to that of the specimen. The rate of rise and maximum temperature reached were determined. Alternatively, by maintaining a certain difference of temperature between the specimen and the calorimeter, it was possible to study rates of release under conditions of finite heat transfer, which simulated those in a reactor.

Further development of the calorimeter made it possible to measure the rate of release of energy at a linear rate of rise of temperature up to 600 °C. The size of specimen most frequently used was a cylinder 0·5 in. by 0·25 in. o.d., but neither the specimen dimensions nor the shape were critical.

The overall accuracy of measurement was $\pm 0{\cdot}01$ cal g^{-1} $degC^{-1}$ ($\pm 2\sigma$) at a rate of rise of 4 degC min^{-1}. Comparisons of results of measurements made on this calorimeter

with those made on the linear-rise and high-temperature linear-rise calorimeters for specimens cut from the same piece of irradiated graphite gave agreement to within $\pm 0{\cdot}01$ cal g^{-1} $degC^{-1}$.

(iii) *Bomb calorimeter*

A detailed description of the isothermal jacket bomb calorimeter used for the total stored energy determinations, together with a full discussion of possible sources of error and their effects on the accuracy of measurement, has been given by Jackson & Cordall (1959). The total stored energy content, which varied from a few calories per gram to several hundred, was determined to within a few parts per cent from the difference between the heat of combustion of the irradiated sample and that of unirradiated graphite (7800 cal g^{-1}). To achieve this precision it was necessary to establish a complete, controlled temperature, boundary to which all heat losses from the calorimeter were referred, and to study the products of combustion so as to eliminate the effects of incomplete combustion of the specimen and of small levels of impurities. Measurements were made on 1 g samples of powdered material.

The estimated standard deviation for heat of combustion measurement on unirradiated graphite was less than $\pm 2{\cdot}5$ cal g^{-1} and this was substantiated by an experimental value of $\pm 1{\cdot}7$ cal g^{-1}, from a series of seven measurements. For the latter value, the estimated accuracy of measurement for a single stored energy determination was better than ± 4 cal g^{-1} ($\pm 2\sigma$). Such an accuracy required full precautions to be taken and for many routine measurements, where adequate sampling was more important than extreme accuracy, conditions were relaxed to give an accuracy of ± 8 cal g^{-1} ($\pm 2\sigma$).

(iv) *Thermal conductivity and electrical resistivity measurements*

Thermal conductivity changes were determined by repeated measurements on samples 3 in. long by 0·25 in. o.d. by the Kohlrausch method. Measurements were made *in vacuo* at a temperature of 25 °C to an accuracy of $\pm 1\,\%$.

The electrical resistivity was determined to an accuracy of $0{\cdot}5\,\%$ at room temperature from the potential drop over the central section of the thermal conductivity specimens when a known current was passed.

3. Calibration of irradiation dose

(*a*) *General considerations*

Calibration experiments had to be made to allow for the neutron spectrum in terms of Calder equivalent temperature, as mentioned in the Introduction. Before they are described, two assumptions which have to be made will be discussed.

The first is that the damaging power of a neutron flux can be expressed by

$$\phi_d = \int_0^\infty \Psi(\epsilon)\,\phi(\epsilon)\,\mathrm{d}\epsilon, \tag{3}$$

where $\phi(\epsilon)\,\mathrm{d}\epsilon$ is the flux of neutrons with energies between ϵ and $\epsilon+\mathrm{d}\epsilon$ and $\Psi(\epsilon)$ is the factor which allows for the variable ability of neutrons of different energies to produce damage. This assumption implies that if graphite samples are irradiated at the

same temperature and for the same time in two neutron fluxes with different energy spectra, but with the same damage flux, they will be damaged identically. It can be wrong, because neutron collisions do not displace atoms randomly but in groups near the sites of collision. Fast neutrons produce large groups and slow neutrons small groups. There are reasons, however, for supposing that in graphite the effect of grouping is unimportant. Thermal agitation causes the displaced atoms to form complex groups of interstitial atoms. Their motion is largely confined to two dimensions because of the high activation energy for penetrating the layer planes. This effect, together with the fact that the initial groups in substances of low atomic weight such as graphite are spread over a large volume, should make the final arrangement of interstitial complexes independent of the initial grouping, particularly when the initial groups overlap as in heavily irradiated samples.

Experiments made in the BEPO reactor at Harwell also suggest that grouping is unimportant. In these, samples of graphite were irradiated in a hollow fuel element and in an empty fuel element channel, thus providing neutron energy spectra differing as much as possible in the core of a graphite-moderated reactor. The irradiations were made at approximately the same temperature, 20 to 30 °C, and the respective rates of change of a number of properties were compared. The ratio was substantially the same for all properties measured, namely electrical resistivity, Young's modulus, thermal conductivity, stored energy and dimensional changes; and independent of dose over a wide range.

The second assumption concerns the effect of the rate at which the damage is produced. The displaced atoms pass through a sequence of configurations which depend on the rate of displacement (i.e. on the damage flux) and on the rate of annealing (i.e. on the temperature). If the damage flux is increased and at the same time the temperature raised so as to increase the annealing rate equally, the sequence of configurations is unchanged but is passed through more quickly. The necessary change in temperature can be determined from the activation energy for annealing Q; thus

$$\frac{1}{\theta_1}-\frac{1}{\theta_2}=\frac{k}{Q}\ln\frac{(\phi_d)_2}{(\phi_d)_1}, \tag{4}$$

where θ_1 is the absolute temperature for the flux $(\phi_d)_1$ and θ_2 is that for $(\phi_d)_2$. An objection to this argument is that there is not one particular activation energy for annealing but a distribution of energies. However, the annealing involves a sequence of processes in which each set of configurations of the displaced atoms is produced from the previous one and there is evidence to suggest that the annealing sequence is controlled by the initial behaviour. Thus the amount of damage is determined by the activation energy during the initial stage of annealing.

If the two assumptions are valid, irradiations with different neutron spectra at different rates of damage have the same effect on the graphite provided that θ_1 and θ_2 are related by equation (4) and that $(\phi_d)_1 t_1 = (\phi_d)_2 t_2$ where t_1 and t_2 are the durations of the irradiations. By adopting suitable standards the specification of the irradiation conditions can be reduced to two quantities, the equivalent temperature and the irradiation dose $\phi_d t$.

These assumptions were used to provide an initial calibration of the test reactor in terms of the dose in a power-producing reactor. Subsequently they were checked by

comparing the stored energy produced in the Calder reactors during the first 2 or 3 years operation with the predicted stored energy obtained from the results of the test reactor experiments.

(*b*) *Calibration experiments*

If both $\Psi(\epsilon)$ and $\phi(\epsilon)$ were known it would be possible to determine the relative damaging power of different reactors from equation (1). Because $\phi(\epsilon)$ is not known experimentally, it was calculated (S. B. Wright, private communication) by the Monte Carlo

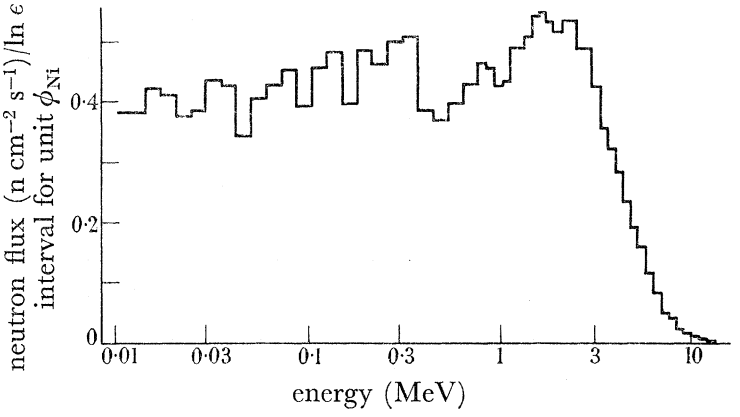

FIGURE 3. Neutron energy spectrum in a hollow fuel element.

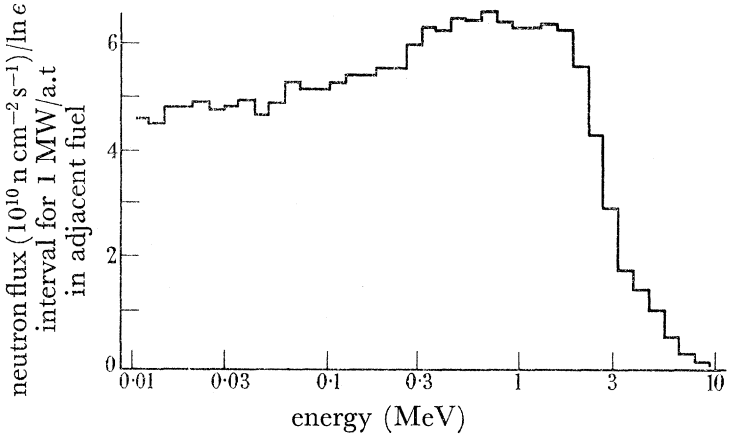

FIGURE 4. Neutron energy spectrum at the wall of a fuel channel in Calder.

method for two of the irradiation positions considered in this work. The results are shown in figures 3 and 4, in which the spectra are normalized to the dose parameters used in this paper, i.e. to ϕ_{Ni} for the test reactor fuel element and to the adjacent fuel rating in the Calder reactor. The ratio of ϕ_d to the dose measurement parameters was determined from resistivity changes on samples $\frac{1}{4}$ in. diameter and 3 in. long irradiated in groups of three, one of high, one of low and one of medium resistivity to remove bias due to variations in the material.

An experiment was made in BEPO to obtain the temperature dependence of resistivity changes. For this purpose graphite specimens of grade *A* and grade *B* (an older type of reactor graphite) were irradiated in two thermostats in a vertical hole in BEPO (T.E. 10). Changes

in resistivity and the Ni doses, $\phi_{\mathrm{Ni}}t$, were measured. The Ni flux was $0{\cdot}9\times10^{11}$ n cm^{-2} s^{-1}. The results were expressible in the form

$$\left.\begin{aligned} x_A = (\rho/\rho_0 - 1)_A &= 0{\cdot}162\,(1-0{\cdot}00514\,T)\,(\phi_{\mathrm{Ni}}t\times10^{-16})^{0{\cdot}75},\\ x_B &= 0{\cdot}633\,(1+0{\cdot}000775\,T)\,x_A, \end{aligned}\right\} \qquad (5)$$

where T is the irradiation temperature in °C, ρ_0 is the resistivity before irradiation, ρ is the resistivity after irradiation, ϕ_{Ni} is the nickel flux (cm^{-2} s^{-1}) and t is the duration of the irradiation in seconds. Measured values of x are compared with equation (5) in figure 5. ϕ_d was defined by putting $\phi_d = \phi_{\mathrm{Ni}}$ in equation (5), with T equal to the equivalent temperature for a flux of $0{\cdot}9\times10^{11}$ n cm^{-2} s^{-1}. To determine ϕ_d in another reactor

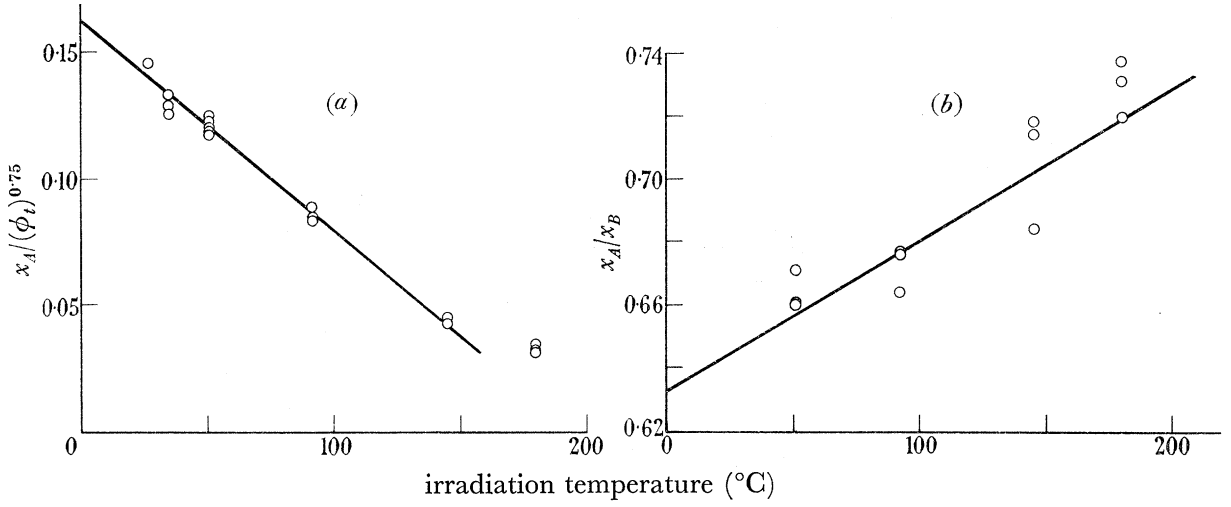

FIGURE 5. (*a*) Temperature dependence of resistivity change (grade *A* graphite).
(*b*) Comparison of resistivity change in grades *A* and *B* graphites.

position x_A or x_B, T, and t were measured. Substitution in equation (5) gave an approximate value ϕ'_d for the damage flux and an approximate equivalent temperature $T'_{\mathrm{eq.}}$ was then obtained from equation (4) by putting $\theta_1 = T+273$, $\theta_2 = T'_{\mathrm{eq.}}+273$, $(\phi_d)_1 = \phi'_d$, and $(\phi_d)_2 = 0{\cdot}9\times10^{11}$. $T'_{\mathrm{eq.}}$ could then be used to obtain a better value for ϕ_d and further iteration can be carried out where necessary. The value of Q was obtained from a separate experiment described later.

A second experiment consisted of measuring ϕ_d and comparing it with the flux derived from activation of Ni, in the following positions in PLUTO:

(*a*) Inside a hollow fuel element with a stainless-steel thimble in the fuel element, site C_4.
(*b*) Inside a hollow fuel element with a stainless-steel thimble in the fuel element, site D_3.
(*c*) Inside a hollow fuel element with an aluminium thimble in the fuel element, site C_4.
(*d*) Inside a stainless-steel thimble in an empty fuel element position at reactor site D_3.

In each position groups of three grade *B* specimens were irradiated at five places along the thimble. In these experiments the reactor was operated at low power, 300 kW, to reduce the correction for equivalent temperature. At this power level temperature control was unnecessary, but temperature measurements were made at each position through the experiments. The results are given in table 3.

These show that the ratio ϕ_d/ϕ_{Ni} is the same for both positions C_4 and D_3, and that it was the same inside steel and aluminium thimbles. Furthermore, this ratio differs by only 20% between these positions inside a fuel element and in an empty fuel element position. In view of this small variation for extreme conditions we may expect the ratio in a fuel element to be independent of minor operational variables such as the loading of the reactor, and the position of the control arms. ϕ_{Ni} can therefore be regarded as a good monitor for graphite damage in this particular case.

TABLE 3. DAMAGE FLUX MEASUREMENTS IN PLUTO AT 300 kW

distance above c/l of reactor (cm)	$10^{-12}\phi_{Ni}$ (cm^{-2} s^{-1})	$10^{-12}\phi_d$ (cm^{-2} s^{-1})	ϕ_d/ϕ_{Ni}
(*a*) Position C_4: inside fuel element with stainless-steel thimble			
23·8	0·62	0·313	0·506
14·8	0·95	0·462	0·487
4·4	1·20	0·622	0·518
−5·7	1·36	0·668	0·492
−14·8	1·39	0·648	0·466
			mean 0·494 ± 0·009
(*b*) Position D_3: inside fuel element with stainless-steel thimble			
23·2	0·48	0·262	0·547
14·1	0·81	0·410	0·505
3·5	1·10	0·514	0·468
−6·7	1·23	0·573	0·466
−15·9	1·24	0·551	0·444
			mean 0·486 ± 0·018
(*c*) Position C_4: inside fuel element with aluminium thimble			
23·8	0·76	0·357	0·469
14·8	1·06	0·529	0·497
4·4	1·37	0·697	0·507
−5·7	1·55	0·747	0·481
−14·8	1·59	0·749	0·471
			mean 0·483 ± 0·008
(*d*) Position D_3: in empty fuel element			
23·2	0·122	0·079	0·646
14·1	0·185	0·114	0·616
3·5	0·246	0·134	0·564
−6·7	0·284	0·171	0·604
−15·9	0·292	0·158	0·542
			mean 0·594 ± 0·019

Mean ϕ_d/ϕ_{Ni} in fuel element = 0·488 ± 0·012 (σ).

Similar experiments were carried out in a hollow fuel element, in an empty fuel element position, and in a normal lattice position in BEPO giving the results shown in table 4. They show that nickel activation does not provide as good a monitor for graphite damage in a graphite moderated reactor as in a heavy-water reactor. If it is used for this purpose care must be taken to maintain the local conditions constant during an experiment.

The next experiment was the determination of the activation energy for obtaining the equivalent temperature correction. Specimens of grade *A* graphite were irradiated in the top, middle and bottom barrels of a standard rig in PLUTO for a period of 3 h at 150 °C, with the reactor operating at 7·5 MW. Measurements were made of the nickel dose

$\phi_{Ni}t$ and the change in resistivity $x = (\rho/\rho_0) - 1$. Using the factor obtained in the 300 kW run, $\phi_{Ni}t$ was converted to $\phi_d t$. Substitution of $\phi_d t$ and x in equation (5) gave the equivalent temperature $T_{eq.}$. The activation energy was then calculated from equation (4) by putting $\theta_1 = 150 + 273$, $\theta_2 = T_{eq.} + 273$, $\phi_1 = \phi_d$, $\phi_2 = 0{\cdot}9 \times 10^{11}$. The results are shown in table 5. The mean value for the activation energy is 1·58 eV. As this value was required in the low-power calibration of PLUTO, an iterative procedure was necessary.

TABLE 4. DAMAGE FLUX MEASUREMENTS IN BEPO

position	ϕ_d/ϕ_{Ni}
experimental hole T.E. 10	1 (standard)
hollow fuel element	0·43
empty fuel channel (3 positions)	1·00
experimental hole E 2/7	0·75

TABLE 5. DETERMINATION OF ACTIVATION ENERGY

position	resistance change $x = \rho/\rho_0 - 1$	$10^{-17}\,\phi_{Ni}t$ (cm^{-2})	$10^{-17}\,\phi_d t$ (cm^{-2})	$\theta_{eq.}$ (°K)	Q (eV)
top	0·657	3·82	1·86	372	1·36
middle	0·708	4·25	2·08	381	1·82
bottom	0·730	4·12	2·01	376	1·55
					mean 1·58 ± 0·18 (σ)

(c) *Comparison of damage flux in graphite-moderated reactors*

It is not possible to operate the Calder reactors under conditions suitable for determining ϕ_d by the method described in §3 (*b*). Instead an empirical method of calculating ϕ_d was developed. This makes use of a function $(1/r)\,\phi(r)$ which is proportional to the damage rate in an infinite graphite mass at a distance r from an infinite line source of fission neutrons. If we ignore the effect of voids in the graphite structure the rate of damage in a reactor can be calculated by summing the damage due to each fuel channel; thus the damage rate at a point, O, is

$$\phi_d = cW \sum_i \frac{1}{r_i}\,\phi(r_i)$$

where r_i is the increase of O from the ith fuel channel and W is the power rating per unit length of fuel. For standard uranium metal fuels, W is proportional to AP, where A is the area of cross-section of the fuel and P is the power rating in MW/a.t. Thus we can compare two reactors 1 and 2, by putting

$$y = \left(\frac{\phi_d}{P}\right)_2 \Big/ \left(\frac{\phi_d}{P}\right)_1 = \left[A \sum_i \frac{1}{r_i}\phi\,(r_i)\right]_2 \Big/ \left[A \sum_i \frac{1}{r_i}\,\phi\,(r_i)\right]_1. \qquad (6)$$

The effect of voids and of different graphite densities is allowed for by replacing $\phi(r_i)$ by by $\phi(r_g')$ where $r_g' = \rho/\rho_0\, r_g$. r_g is the distance through the graphite from the fuel element, ρ is the density, and ρ_0 is a standard density.

The function $\phi(r)$ has been determined by Kinchin (private communication) by using resistivity changes to measure damage in graphite irradiated at various distances in the reflector of BEPO. His result is shown in figure 6. The ratio y has been calculated for several positions in the Calder reactors using the centre of a lattice cell in BEPO as a standard position. The positions are shown in figure 7 and results are given in table 6.

To establish the Calder equivalent flux in MW/a.t corresponding to a given Ni flux in the test reactors, we determine the ratio ϕ_d/P for the centre of a lattice cell in BEPO. Two methods have been used for this purpose. In both ϕ_d was measured as described in §3 (*b*). In the first, P was determined from the total power of the reactor and the variation

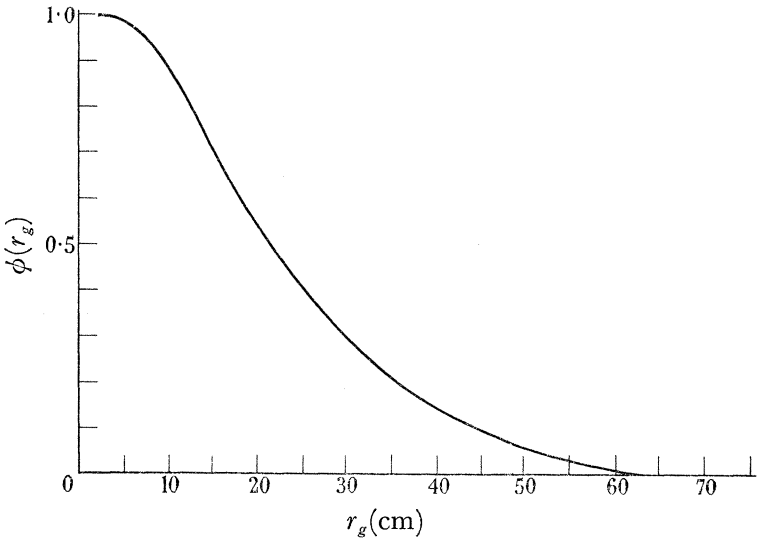

FIGURE 6. Variation of damage with distance through graphite.

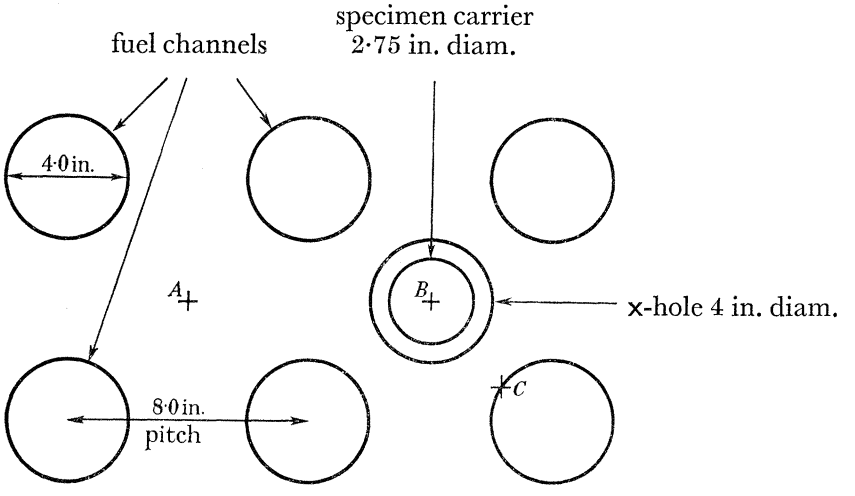

FIGURE 7. Positions in the Calder lattice. *A*, centre of lattice; *B*, x-hole specimen carrier; *C*, fuel channel wall.

TABLE 6. COMPARISON OF DAMAGE FLUX BETWEEN BEPO AND CALDER PER UNIT POWER RATING

position	A (cm^2)	$\Sigma 1/r(\phi(r))$	y
BEPO	4·1	1·13	1
A Calder centre of lattice	6·66	0·94	1·37
B Calder x-hole specimen carrier	6·66	1·02	1·48
C Calder fuel channel wall	6·66	1·32	1·91

of flux through the reactor, as was done in the case of Calder reactors. In the second P was found by measuring the thermal flux $\phi_{\text{th.}}$ and calculating P from the relation $P = 3{\cdot}25 \times 10^{-13} \alpha f \phi_{\text{th.}}$ where α is the ratio of the mean flux in the uranium to the flux at the standard position in the graphite; f is a factor allowing for fast fission, usually about 1·03. These methods have been used for various positions in BEPO and in the Windscale reactors. The Windscale results can be applied to BEPO by making use of equation (6). Results for ϕ_d/P in BEPO are collected in table 7.

TABLE 7. DAMAGE FLUX PER UNIT POWER RATING IN BEPO

	$10^{-11}\phi_d/P$ (cm^{-2} s^{-1} per MW/a.t)		
position	method (*a*)	method (*b*)	mean
early work, BEPO	3·23	3·73	3·54
Windscale	3·40	3·80	
present work			
T.E.10 (1)	2·70	1·98	2·55
(2)	3·23	2·32	
E 2/7	1·90	1·94	
weighted mean			2·8

The main reason for the scatter of these experiments is that the thermal flux is easily perturbed by neutron absorption in the neighbourhood of the experiments. It is difficult to make an experiment under unperturbed conditions in a heavily used reactor such as BEPO. It is considered that the best value for ϕ_d/P in BEPO is $2{\cdot}8 \times 10^{11}$ n cm^{-2} s^{-1} per MW/a.t.

Using this result, together with the data in tables 3 and 6, the values in table 8 are obtained for the MW/a.t in Calder equivalent to unit Ni flux in the test reactor and for the positions shown in figure 7.

TABLE 8. CALCULATION OF EQUIVALENT MWD/A.T FOR DIFFERENT SITES

position	MWd/a.t
A, centre of lattice	0·72 × integrated power rating in adjacent fuel
B, x-hole specimen carrier	0·78 × integrated power rating in adjacent fuel
B, fuel channel wall	equal to integrated power rating in adjacent fuel
material testing reactor	$1{\cdot}06 \times 10^{-17}\ \phi_{\text{Ni}}\, t$

(*d*) *Determination of* ϕ_{Ni} *in high flux irradiations*

It was shown in §3 (*b*) that Ni activation by the reaction ^{58}Ni (n, p) ^{58}Co provides a good monitor for irradiation damage in graphite irradiated in the material-testing reactors. Although this activation can be measured very well for the small doses used in the calibrations, its use as a monitor in the high flux irradiations is much more difficult, partly because of the short half-life of ^{58}Co and partly because of the interfering effect of the thermal neutron reaction ^{58}Co (n, γ) ^{59}Co. Doses in the high-flux reactors have therefore been determined by measuring the thermal flux using the reaction ^{59}Co (n, γ) ^{60}Co and making a separate study of the ratio $\phi_{\text{Ni}}/\phi_{\text{Co}}$ for a variety of reactor conditions. It was found that the only factor which significantly affected this ratio in the region of the core used in the graphite irradiations was the amount of uranium in the fuel element surrounding the specimens. In the course of this work two types of fuel elements have been used, one containing 115 g of ^{235}U and one containing 150 g of ^{235}U. The quantity of uranium in the

fuel element also varies considerably during operation as the fuel is used up. Measurements of the ratio ϕ_{Ni}/ϕ_{Co} as a function of burn-up gave the following results:

for 115 g *elements* $\phi_{Ni}/\phi_{Co} = 0{\cdot}378$ to $0{\cdot}404\,b$,

for 150 g *elements* $\phi_{Ni}/\phi_{Co} = 0{\cdot}502$ to $0{\cdot}530\,b$,

where b is the fraction of fuel burned. b was determined before and after each period of irradiation and the mean value used to calculate ϕ_{Ni} from the thermal flux. $\phi_{Ni}t$ was then converted to the equivalent MWd/a.t for Calder by means of the factor derived in §3(*c*). A small correction was included to allow for the fact that the position of the dose monitor was not exactly the same as that of the specimens.

4. Experimental data

A large number of measurements have been made of rate of release of stored energy, total stored energy and thermal conductivity on specimens from the rigs and from Calder. In some cases the measurements themselves were known to be of doubtful accuracy, e.g. because of an instability in the linear-rise calorimeter during the measurement. In other

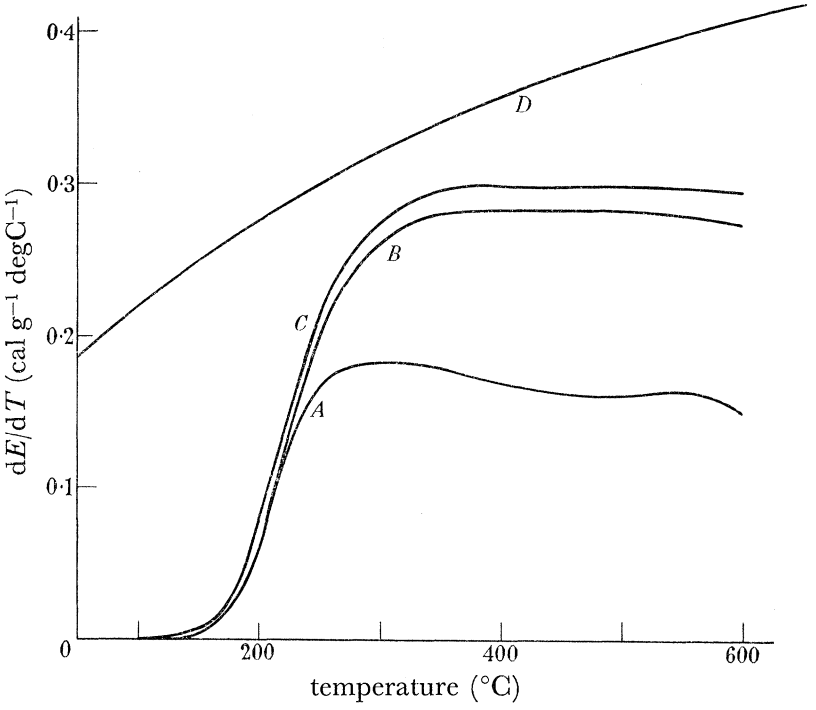

Figure 8. Rate of release of stored energy in specimens irradiated in 150 °C rig. *A*, 2000 MWd/a.t; *B*, 7735 MWd/a.t; *C*, 11320 MWd/a.t; *D*, specific heat of unirradiated graphite.

cases, critical analysis of the knowledge of irradiation temperature revealed that the possible error in the estimate was large or large variations had occurred during irradiation; this was so for many of the Calder specimens. All data on which there was reason to doubt the accuracy have been excluded.

A few curves for dE/dT are shown in figures 8 and 9. In figure 8 the curves are for specimens irradiated at a rig temperature of 150 °C to three different doses. In figure 9

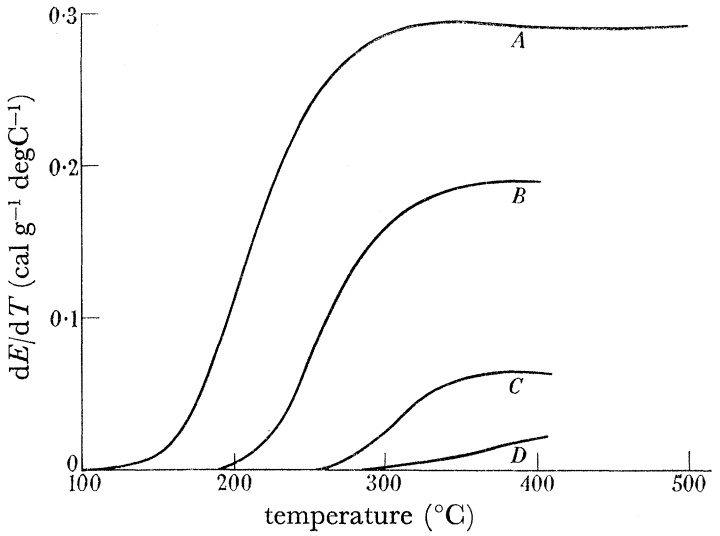

FIGURE 9. The effect of equivalent irradiation temperature on the rate of release of stored energy. *A*, 5015 MWd/a.t at 135 °C; *B*, 5300 MWd/a.t at 180 °C; *C*, 4835 MWd/a.t at 223 °C; *D*, 4100 MWd/a.t at 269 °C.

TABLE 9. DATA FOR SPECIMENS IRRADIATED IN 150 °C RIG

Specimen temperature: 155 °C, actual; 135 °C, Calder equivalent

positions in rig	periods	dose: nickel $\times 10^{-20}$	dose: MWd/a.t	$\frac{K_0}{K}-1$	E (cal g^{-1})	$(dE/dT)_{400}$ (cal g^{-1} degC^{-1}): expt.	$(dE/dT)_{400}$ (cal g^{-1} degC^{-1}): empirical
*T*1	1	0·586	620	18·6	—	—	0·072
*T*8	1	0·586	620	18·0	—	—	0·070
*T*8	2	0·654	690	16·2	—	—	0·063
*B*8	1	0·675	715	17·2	—	—	0·067
*M*8	1	0·714	755	19·8	—	—	0·077
*B*8	2	0·797	845	—	151	—	0·094
*M*8	2	0·817	865	—	170	—	0·106
*T*8	1, 3	1·20	1270	33·6	—	—	0·130
*T*1	2, 3	1·27	1345	33·0	—	—	0·128
*B*8	1, 3	1·38	1460	37·9	—	—	0·148
*M*2	1, 2	1·53	1620	34·2	274	—	0·169
*T*1	4, 5	1·69	1790	28·6	—	—	0·111
*T*5	1–3	1·85	1960	52·6	302	—	0·184
*T*3	1–3	1·85	1960	38·3	—	—	0·149
*M*7; *M*9	6; 7	1·89	2000	46·5	—	0·170	—
*M*7	4, 5	2·11	2235	68·1	—	—	0·243
*M*1*a*	4, 5	2·11	2235	—	373	—	0·219
*M*2*a*	4, 5	2·11	2235	—	387	—	0·226
*B*1	1–3	2·18	2310	—	336	—	0·201
*B*5	1–3	2·18	2310	—	334	—	0·200
*B*7	1–3	2·18	2310	44·0	—	—	0·169
*B*3	1–3	2·18	2310	50·1	—	—	0·190
*T*8	2, 4, 5	2·34	2480	—	352	—	0·208
*B*4	8, 9	2·54	2690	57·2	—	—	0·211
*B*6	8, 9	2·54	2690	58·5	—	—	0·215
*T*9*a*; *M*9*a*	2, 4, 5; 8	2·96	3135	—	—	0·235	—
*T*3	1–5	3·54	3750	59·0	—	—	0·217
*B*7; *B*1	1–3; 4–5	4·17	4420	68·2	—	—	0·243
*B*3	1–5	4·17	4420	70·0	—	—	0·250
*B*4*a*	1–5	4·17	4420	—	469 474	—	0·260 0·262
*M*3*b*; *M*8*a*	4–5; 8–9	4·73	5015	—	—	0·292	—
*B*3; *B*1	1–5; 7	5·36	5680	—	560	0·277	—
*B*6*b*; *T*2*b*	1–5; 7–9	7·30	7735	—	—	0·282	—
*B*2*b*; *M*2*b*; *B*2*a*	1–5; 7–9 10–12	10·68	11320	—	—	0·306	—

the curves are for specimens irradiated to similar doses at different rig temperatures. The large effect of irradiation temperature is clearly seen. From each dE/dT curve the value at 400 °C was selected as representative. These $(dE/dT)_{400}$ values are given in the tables of results.

TABLE 10. DATA FOR SPECIMENS IRRADIATED IN 200 °C RIG

Specimen temperature: 205 °C, actual; 180 °C, Calder equivalent.

positions in rig	periods	dose: nickel $\times 10^{-20}$	dose: MWd/a.t.	$\frac{K_0}{K}-1$	E (cal g^{-1})	$(dE/dT)_{400}$ (cal g^{-1} degC^{-1}): expt.	$(dE/dT)_{400}$ (cal g^{-1} degC^{-1}): empirical
*T*1	1	0·695	735	11·8	—	—	0·46
*T*5	1	0·695	735	—	82 85	— —	0·051 0·053
*T*8	1	0·695	735	10·5	—	—	0·041
*B*8	1	0·927	980	15·0	—	—	0·058
*M*8	1	0·932	985	13·5	—	—	0·053
*T*1	2, 3	1·51	1600	17·7	—	—	0·069
*T*8	2, 3	1·51	1600	16·7	—	—	0·065
*B*1	1, 2	1·58	1675	14·7	—	—	0·057
*B*2	1, 2	1·58	1675	20·6	—	—	0·080
*B*8	1, 2	1·58	1675	12·6	—	—	0·049
*B*3	1, 2	1·58	1675	14·5	—	—	0·056
*B*9	1, 2	1·58	1675	12·8	—	—	0·050
*B*5	1, 2	1·58	1675	13·4	—	—	0·052
*B*6	1, 2	1·58	1675	12·3	—	—	0·048
*B*8	2, 3	1·67	1770	19·8	—	—	0·077
*M*8	2, 3	1·70	1800	20·9	149	—	0·093
*M*9*a*	2, 3, 5	2·24	2375	—	—	0·104 0·106	— —
*B*1	1–3	2·60	2755	27·9	203	—	0·127
*B*8	1, 4	2·73	2890	32·7	—	—	0·127
*B*9	1, 4	2·73	2890	—	181	0·119 0·118	— —
*M*8	1, 4	2·76	2925	31·1	—	—	0·121
*T*8	2, 3, 5–7	3·00	3180	29·3	—	—	0·114
*T*1; *M*8	2, 3; 5–7	3·42	3625	35·2	—	—	0·137
*B*8	2, 3, 5–7	3·57	3785	38·7	—	—	0·148
*B*7	1–4	4·40	4665	48·9	—	—	0·186
*M*6	1, 2–4	4·46	4730	—	270	0·171 0·190	—
*M*2	1, 2–5	5·00	5300	58·7	328	0·189 0·179	—
*M*5	1–8, 10–12	8·67	9190	—	—	0·20	—
*B*8; *M*8	1, 4, 8–15; 16, 17	9·23	9785	92·0	—	—	0·294
*B*5	1–15	11·86	12570	—	—	0·24	—
*M*4; *T*8	1–12, 14, 15, 16, 17	11·93	12645	79·5	—	—	0·271

Tables 9 to 13 show the data from the irradiation rigs. The temperature quoted for the rig is the nominal value at which it was controlled; the actual irradiation temperature was taken as 5 degC higher than this on the basis of the heat transfer calculations mentioned earlier. The column showing the 'position in rig' is given for interest, *T* is the top, *M* the middle and *B* the bottom barrel of the rig, and the number is the hole reference. The 'period' column is again for interest and shows the reactor periods (of roughly 6 weeks each) for which the specimen was in pile. The dose was determined experimentally using $^{59}Co(n, \gamma)\ ^{60}Co$. The nickel dose and Calder equivalent figures were calculated from this

following the methods described in §3 (*d*) and in table 8. From a knowledge of the total dose and the time the reactor was at power, the average power rating was determined. This was used in equation (4) to determine the Calder equivalent temperature for the 'standard' rating of 3·12 MW/a.t and an activation energy of 1·58 eV (table 5). In practice this varies by up to 7 degC from one period to another because of changes in reactor power, but the selection of a mean value for all specimens is sufficiently accurate.

TABLE 11. DATA FOR SPECIMENS IRRADIATED IN 250 °C RIG

Specimen temperature: 255 °C, actual; 223 °C, Calder equivalent.

positions in rig	periods	dose: nickel $\times 10^{-20}$	dose: MWd/a.t	$\frac{K_0}{K}-1$	E (cal g^{-1})	$(dE/dT)_{400}$ (cal g^{-1} degC^{-1}): expt.	$(dE/dT)_{400}$ (cal g^{-1} degC^{-1}): expirical
*M*8	*f*2	0·375	395	—	40	—	0·025
*T*1	1	0·762	805	5·50	29	—	0·018
*T*8	1	0·762	805	5·99	—	—	0·023
*B*8	1	0·967	1025	5·54	—	—	0·022
*M*8	1	0·970	1030	6·52	—	—	0·025
*M*8	*f*2, 3	1·24	1315	6·79	—	—	0·026
*M*2	1, *f*2	1·35	1430	6·85	—	—	0·027
*M*6	1, *f*2	1·35	1430	10·1	—	—	0·039
*M*4	1, *f*2	1·35	1430	7·89	—	—	0·030
*B*8	2–3	1·51	1600	7·77	—	—	0·030
*T*2*a*	5, 6	1·70	1800	—	—	0·032 0·032	— —
*T*8	1, 5, 6	2·46	2610	9·75	—	—	0·038
*B*1	1–3	2·48	2630	10·6	—	—	0·041
*B*5	1–3	2·48	2630	12·3	—	—	0·048
*B*7	1–3	2·48	2630	11·1	79	0·045	—
*B*3	1–3	2·48	2630	11·0	—	—	0·043
*M*8; *T*8; *M*8	1; 4; 5	2·78	2945	14·4	—	—	0·056
*B*8	1, 5, 6	3·05	3235	12·5	—	—	0·048
*M*2; *T*2; *M*2	1–3; 4; 5	4·39	4655	16·7	—	—	0·065
*M*6; *T*6 *M*6	1–3; 4; 5	4·39	4655	16·4	—	—	0·064
*M*4; *T*4; *M*4	1–3; 4; 5	4·39	4655	16·9	—	—	0·066
*B*6*a*	1–3, 5, 6	4·56	4835	—	122	0·066 0·062	— —
*M*2; *T*2; *M*2	1–3; 4; 5, 6	5·19	5500	19·21	146	0·072 0·072	— —
*M*1; *T*1; *M*1	1–3; 4; 5–8	7·39	7835	—	—	0·080	—

TABLE 12. DATA FOR SPECIMENS IRRADIATED IN 300 °C RIG

Specimen temperature: 305 °C, actual; 269 °C, Calder equivalent.

positions in rig	periods	dose: nickel $\times 10^{-20}$	dose: MWd/a.t	$\frac{K_0}{K}-1$	E (cal g^{-1})	$(dE/dT)_{400}$ (cal g^{-1} degC^{-1}): expt.	$(dE/dT)_{400}$ (cal g^{-1} degC^{-1}): empirical
*B*8; *T*8	3; 4	0·792	840	2·61	—	—	0·010
*B*8	1, 2	1·77	1875	5·90	—	—	0·023
*B*7	1, 2	1·77	1875	5·27	31	—	0·019
*B*4*b*	1–3	2·15	2280	—	40	—	0·025
*B*6*a*; *T*6*a*	1–3; 4	2·56	2715	—	42	—	0·026
*B*1; *T*1	1–3; 4	2·56	2715	9·11	—	—	0·035
*B*3; *T*3	1–3; 4	2·56	2715	5·70	—	—	0·022
*B*4; *T*4; *M*4; *T*4	1–3; 4; 5; 6	3·87	4100	—	—	0·022 0·018	— —
*B*1; *T*1; *M*1; *T*1	1–3; 4; 5; 6	3·87	4100	10·7	—	—	0·042
*B*5; *T*5; *M*5; *T*5	1–3; 4; 5; 6	3·87	4100	10·9	—	—	0·042
*B*3; *T*3; *M*3; *T*3	1–3; 4; 5; 6	3·87	4100	7·0	—	—	0·027

The appropriate mean is quoted in each table. The values determined experimentally for the change in thermal conductivity $(K_0/K-1)$, for total stored energy (E) and for $(\mathrm{d}E/\mathrm{d}T)_{400}$ are shown. The final column gives values for $(\mathrm{d}E/\mathrm{d}T)_{400}$ obtained by empirical correlations with other thermal conductivity changes and with total stored energy described in §5.

TABLE 13. DATA FOR SPECIMENS IRRADIATED IN 350 °C RIG

Specimen temperature: 355 °C, actual; 314 °C, Calder equivalent.

positions in rig	periods	dose: nickel $\times 10^{-20}$	dose: MWd/a.t	$\frac{K_0}{K}-1$	E (cal g^{-1})	$(\mathrm{d}E/\mathrm{d}T)_{400}$ (cal g^{-1} degC^{-1}): expt.	$(\mathrm{d}E/\mathrm{d}T)_{400}$ (cal g^{-1} degC^{-1}): empirical
*T*8	2	0·645	680	1·66	17	—	0·011
*T*1	1	0·666	705	1·76	1	—	0·001
*T*8	1	0·666	705	1·85	—	—	0·008
*B*8	1	0·792	840	2·11	—	—	0·008
*M*8	2	0·795	840	—	38	—	0·024
*M*8	1	0·809	860	2·43	—	—	0·009
*T*1	4, 5	1·15	1220	2·72	—	—	0·011
*T*8	4, 5	1·15	1220	2·90	—	—	0·011
*T*1	2, 3	1·46	1550	2·90	—	—	0·011
*T*8	1, 3	1·48	1570	2·81	—	—	0·011
*M*1 *a*	1, 2	1·60	1695	—	22	—	0·014
*M*8	1, 3	1·77	1875	3·18	—	—	0·012
*T*3	1–3	2·12	2245	3·54	—	—	0·014
*T*7	1–3	2·12	2245	2·74	26	—	0·016
*B*8; *M*8	1, 4, 5	2·15	2280	4·38	—	—	0·017
*M*1	3, 4, 5	2·32	2460	4·66	29	—	0·018
*M*2	1–3	2·56	2715	—	41	—	0·025
*M*6	1–3	2·56	2715	3·79	—	—	0·015
*T*8	1, 3, 6, 7	2·80	2970	3·60	—	—	0·014
*T*3	1–5	3·27	3365	5·16	32	—	0·020
*M*8	1, 3, 6, 7	3·39	3590	4·43	—	—	0·017
*B*8; *M*8; *M*8	1, 4, 5, 9–15; 16, 17	7·78	8245	8·60	—	—	0·034
*M*2; *B*9; *T*9; *B*9, *B*9	4–7; 9–13; 14; 15; 16, 17	8·42	8925	6·70	—	—	0·026
*T*5; *T*7; *M*1, *M*1	1–7; 8; 9–15; 16, 17	10·63	11265	9·38	—	—	0·037
*M*6; *T*4; *B*1; *T*1; *B*1; *B*1	1–7; 8; 9–13; 14; 15; 16, 17	11·38	12060	9·77	—	—	0·038

The data from Calder specimens are shown in table 14. The first four columns are presented for general interest. The fourth describes the position of the specimen; *C* is a container specimen, *B* is a specimen cored from a moderator brick, and the number indicates which container or brick, counting from the bottom, is involved. The actual irradiation temperatures are mostly estimated from the curves shown in figure 1, although a few are from thermocouple results on a neighbouring dummy specimen. The doses and the flux data are obtained by the methods described in §2(*a*). The equivalent dose for specimens taken from a fuel channel are the same as calculated; for specimens from x-holes they are obtained from the relations given in table 8 (the actual value there quoted is for x-holes in zone *A*, whereas for those in other zones a slightly different value is appropriate). The equivalent temperatures are again determined using equation (4) and 1·58 eV. Again, in addition to values of $(\mathrm{d}E/\mathrm{d}T)_{400}$ determined directly, those deduced from E by empirical methods are also quoted.

PHILOSOPHICAL TRANSACTIONS OF THE ROYAL SOCIETY A MATHEMATICAL, PHYSICAL & ENGINEERING SCIENCES

TABLE 14. DATA FOR SPECIMENS IRRADIATED IN CALDER HALL

reactor	channel	shut-down	position	irradiation temperature (°C)	equiuvalent irradiation temperature (°C)	dose	equivalent dose (MWd/a.t)	total stored energy, E (cal g^{-1})	$(dE/dT)_{400}$ (cal g^{-1} degC^{-1}) experimental	$(dE/dT)_{400}$ (cal g^{-1} degC^{-1}) empirical
1	12/26 *X*	Aug. 1957	*C*2	154	182	120	85	18	—	0·011
1	07/26 *X*	Nov. 1957	*C*3	162	170	720	560	72	—	0·043
2	07/26 *X*	Jan. 1958	*C*2	162	174	450	350	58	—	0·035
1	07/26 *X*	July 1958	*C*2	153	163	780	605	46	0·057	0·028
1	07/26 *X*	July 1958	*C*3	162	170	1060	820	—	0·044	—
1	09/26 *X*	July 1958	*C*2	153	167	670	480	44	0·045	0·026
1	09/26 *X*	July 1958	*C*3	162	173	900	645	70	—	0·043
1	10/25 *X*	July 1958	*C*2	150	167	500	358	47	0·048	0·028
1	11/26 *X*	July 1958	*C*2	154	174	430	310	43	0·043	0·025
1	12/26 *X*	July 1958	*C*2	154	183	195	140	16	0·024	0·010
1	07/26 *R*	July 1958	*B*2	175 ± 6	180	1230	1230	—	0·062	—
1	07/26 *R*	July 1958	*B*3	202 ± 8	205	1440	1440	—	0·042	—
1	07/26 *R*	July 1958	*B*8	306 ± 11	338	410	410	—	0·00	—
2	12/26 *X*	Oct. 1958	*C*2	154	182	205	145	—	0·020	—
1	07/26 *R*	May 1959	*B*1	147 ± 4	155	1070	1070	—	0·083	—
1	07/26 *R*	May 1959	*B*1	147 ± 4	155	1070	1070	93*	0·072	0·056
1	07/26 *R*	May 1959	*B*2	169 ± 5	175	1580	1580	—	0·085	—
1	07/26 *R*	May 1959	*B*2	169 ± 5	175	1580	1580	110*	0·081	0·066
1	07/26 *R*	May 1959	*B*3	197 ± 10	200	2030	2030	101*	0·050	0·060
1	07/26 *R*	May 1959	*B*4	225 ± 10	227	2200	2200	74*	0·042	0·044
1	07/26 *R*	May 1959	*B*5	253 ± 12	256	2020	2020	39*	0·022	0·023
3	12/26 *X*	July 1959	*C*7	190*a* ± 5	209	290	206	—	0·010	—
2	07/26 *R*	Aug. 1959	*B*1	157 ± 4	163	1290	1290	—	0·077	—
2	07/26 *R*	Aug. 1959	*B*3	211 ± 6	212	2170	2170	101*	0·053	0·060
2	07/26 *R*	Aug. 1959	*B*4	242 ± 7	244	2240	2240	77*	0·029	0·047
2	07/26 *R*	Aug. 1959	*B*5	268 ± 7	270	2080	2080	—	0·015	—
2	07/26 *R*	Aug. 1959	*B*6	290 ± 8	298	1460	1460	22*	0·006	0·013
1	08/23 *X*	Apr. 1960	*C*2	153	167	295	211	—	0·046	—
1	08/23 *X*	Apr. 1960	*C*3	160*a*	169	375	270	57	0·060	0·035
1	08/23 *X*	Apr. 1960	*C*4	169	175	460	330	—	0·042	—
1	08/23 *X*	Apr. 1960	*C*5	182*a*	187	545	390	—	0·040	—
1	08/23 *X*	Apr. 1960	*C*6	192	197	615	440	—	0·033	—
1	08/23 *X*	Apr. 1960	*C*7	205*a*	208	615	440	—	0·025	—
1	08/23 *X*	Apr. 1960	*C*8	219	225	584	420	—	0·021	—
1	08/23 *X*	Apr. 1960	*C*9	236	244	522	373	—	0·020	—
1	08/23 *X*	Apr 1960	*C*10	256*a*	270	435	313	27	0·009	0·016
1	07/26 *K*	Apr. 1960	*B*2	160	167	1580	1580	112*	0·113	0·067
1	07/26 *K*	Apr. 1960	*B*3	184	185	2425	2425	147*	0·108	0·088
1	07/26 *K*	Apr. 1960	*B*4	212	210	2920	2920	138*	0·084	0·083
1	07/26 *K*	Apr. 1960	*B*5	241	239	3090	3090	83*	0·045	0·050
1	07/26 *K*	Apr. 1960	*B*6	272	272	2830	2830	63*	0·048	0·037
1	07/26 *K*	Apr. 1960	*B*7	298	303	2235	2235	44	—	0·027
1	07/26 *K*	Apr. 1960	*B*8	316	334	1570	1570	53*	0·010	0·033

a From thermocouple in immediate vicinity. * E and $(dE/dT)_{400}$ on parts of same sample.

In addition to the data from Calder specimens quoted in table 14, other data were collected in which, although the irradiation temperatures of the specimens were not known accurately, E and $(\mathrm{d}E/\mathrm{d}T)_{400}$ were measured on different parts of the same specimen. These are used subsequently and the values are recorded in table 15.

TABLE 15. ADDITIONAL DATA FOR SPECIMENS IRRADIATED IN CALDER HALL WHERE E AND $(\mathrm{d}E/\mathrm{d}T)_{400}$ WERE MEASURED ON PARTS OF THE SAME SPECIMEN

E (cal g^{-1})	$(\mathrm{d}E/\mathrm{d}T)_{400}$ (cal g^{-1} degC^{-1})	E (cal g^{-1})	$(\mathrm{d}E/\mathrm{d}T)_{400}$ (cal g^{-1} degC^{-1})
14	0·008	66	0·034
20	0·021	74	0·042
22	0·006	77	0·029
28	0·013	85	0·064
32	0·025	89	0·065
33	0·028	93	0·072
39	0·022	101	0·053
60	0·042	105	0·072
61	0·033	110	0·081
62	0·070	135	0·080
62	0·079	140	0·098

5. DISCUSSION

(*a*) *Correlation of changes in physical properties*

It is of interest to seek correlations between the three physical properties measured to increase, if possible, the number of results on which an assessment of trends could be based. Previous work (Woods *et al.* 1956) has shown that while the changes in electrical resistance and Young's Modulus quickly saturate with increasing dose, the changes in stored energy (E and $\mathrm{d}E/\mathrm{d}T$), thermal conductivity, lattice spacing changes and macroscopic growth continue to very high doses. The relations between the first three properties in this group are investigated here.

For this purpose it is essential that the comparison be made on specimens whose doses and temperatures are identical; since the variation of physical property change is less sensitive to dose than to temperature the latter is more critical. On the other hand, the actual value of the dose is irrelevant and a knowledge of the temperature is only required to examine whether the correlation between property changes depends on irradiation temperature. These considerations limit the comparison to specimens taken from the rigs, where the irradiation temperatures were controlled accurately, and to Calder specimens where the physical properties were measured on different parts of a single irradiated specimen, as in table 15. No correlation is attempted between one property determined from the rig specimens and a second from Calder material.

The relation between the fractional change of thermal conductivity and total stored energy is shown in figure 10. These results are taken entirely from rigs. The points from the different rigs are differentiated (the points for the higher temperature rigs fall nearer the origin because of the lower damage at these temperatures). It is clear that total stored energy is proportional to the fractional change in thermal conductivity within the range of damage studied, and that for this limited range of irradiation temperatures the proportionality constant is independent of temperature, namely $E = 6{\cdot}25\ (K_0/K - 1)$.

This relation is used below to derive values of E from specimens where only thermal conductivity was measured. Figure 10 also demonstrates the constancy of temperature of specimens in one rig; points marked ′ are obtained by correlation of results from different samples from a rig and show no greater scatter than the other points where both measurements were made on the same sample.

The relation between the total stored energy and rate of release of energy with increasing annealing temperature is shown in figure 11. The majority of the points are from Calder specimens. There is clearly an appreciable scatter and the Calder data have been examined in detail to discover whether the relation between E and $(\mathrm{d}E/\mathrm{d}T)_{400}$ was sensitive to the irradiation temperature. There was no evidence that this was so, as is confirmed by

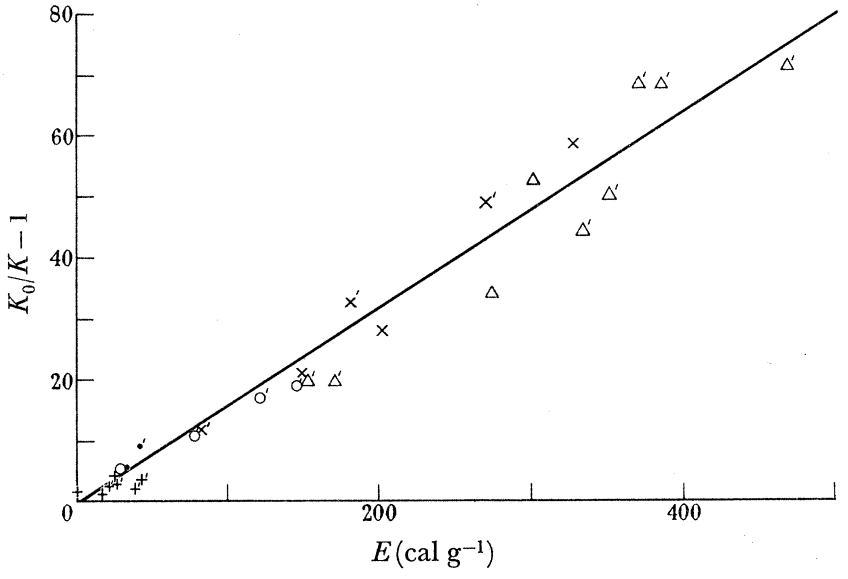

FIGURE 10. Fractional change in thermal conductivity and total stored energy. △, 150 °C rig; × 200 °C rig; ○, 250 °C rig. •, 300 °C rig; +, 350 °C rig; ′ denotes measurements on different specimens.

comparisons between the data from rigs at different temperatures. The scatter is attributed largely to experimental errors of measurement, although temperature gradients in specimens probably contribute. Another noticeable feature is that points for the rigs lie rather lower than those for Calder material, although the results do not overlap sufficiently to be certain that this is significant. This would suggest that the dependence of irradiation damage on temperature is affected by the neutron energy spectrum at high damage levels. The curve shown represents all the data within the scatter (except the Hanford data noted below) but has been biased to give rather more weight to the rig points since these are the more important in the following discussion.

The relation between E and $(\mathrm{d}E/\mathrm{d}T)_{400}$ implies approximately that a total stored energy of 300 cal g^{-1} corresponds to a release rate of 0·18 cal g^{-1} degC^{-1} measured at 400 °C. If the release rate continued uniformly over the whole temperature range, then energy would continue to be released up to temperatures of about 1800 °C. This is a little higher than the annealing temperature necessary to recover physical property changes caused by irradiation. However, unpublished Windscale experiments suggested that there may be a

broad peak in dE/dT at about 1200 °C. Figure 11 also suggests that the dE/dT levels at release temperatures above those of interest in this work build up slowly after $(dE/dT)_{400}$ has saturated at about 0·3 cal g^{-1} $degC^{-1}$.

That the relation between E and $(dE/dT)_{400}$ is not significantly affected by irradiation temperature within the range studied confirms the general impression gained from the dE/dT curves, some of which are shown in figure 8, that the dE/dT value rises uniformly throughout the whole range of annealing temperature as the dose increases. This is quite different from the 'low temperature' (200 °C) peak which rapidly rises at small doses but then changes little with increasing dose while dE/dT at higher temperatures is continuing to rise (Bell & Greenough 1957). The points shown on figure 11 from graphite

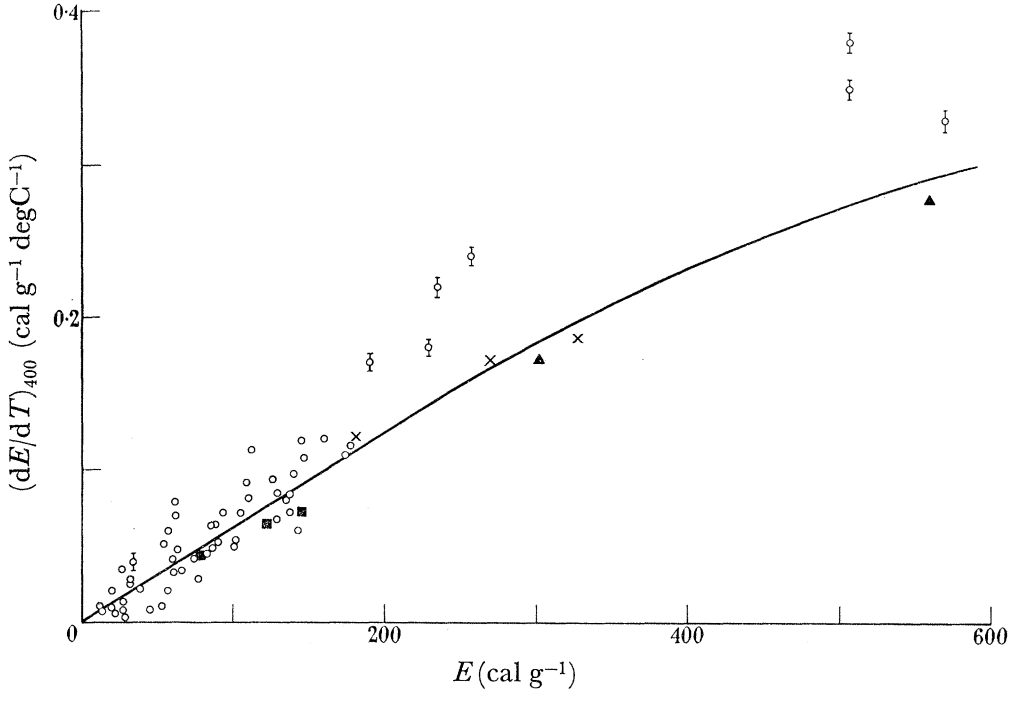

FIGURE 11. Total stored energy and rate of release of stored energy at 400 °C. ○, Calder; ▲, 150 °C rig; ×, 200 °C rig; ■, 250 °C rig; ⊖, Hanford.

irradiated at 30 °C in the Hanford reactors, but measured at Windscale, do not follow the general trend and the difference may indicate that for irradiation temperatures below about 100 °C the mechanism of irradiation damage differs; it could also be related to the small difference between rig and Calder points noted earlier. The Hanford points were ignored in drawing the graph line shown. This graph is used later to derive $(dE/dT)_{400}$ results from values of E derived either by direct experiment or from experimental thermal conductivity values.

The correlation of E and dE/dT shows broadly that the various lattice defects produced by irradiation, which require different activation energies to disperse, all accumulate roughly in a fixed proportion. No theory which supposes that one particular site is preferred for condensation of interstitials until 'full', and that some second site is then filled, could explain this.

(*b*) *Assessment of data for reactor design*

The purpose of the work was to assess the limiting irradiation conditions which would lead to stored energy values which were safe after doses of 30000 to 40000 MWd/a.t in 20 to 30 years for irradiation temperatures in the range 150 to 350 °C. Since no quantitative picture of the basic processes could be deduced from the existing or the new data, and the experiments themselves had not reached the maximum safe values for $(\mathrm{d}E/\mathrm{d}T)_{400} = 0{\cdot}3$ cal g^{-1} degC^{-1} (about) at all temperatures, it was necessary to use empirical methods. The penalties associated with errors are economic and very large; too high a minimum temperature could lead to designs expensive to build and operate; too low a temperature an approach to unsafe conditions before the end of the planned reactor life. While in the latter case irradiation annealing (Nightingale 1957) could be used to extend the life, it involves more severe penalties than the first one, and for design purposes a judicious degree of conservatism is appropriate. This may vary from one design to another; here, to illustrate the general approach, a 'best' estimate is made.

The clearest way of illustrating the data, and of using them for extrapolation, is to show how $(\mathrm{d}E/\mathrm{d}T)_{400}$ increases with increasing dose at various irradiation temperatures. Thus graphs were plotted for each rig temperature to show this. It is clear that the amount of data on $\mathrm{d}E/\mathrm{d}T$ obtained by direct measurement is not large, and that thermal conductivity data preponderate. This is because stored energy measurements, both total and rate of release, are destructive; once a measurement is made the specimen cannot be replaced in a rig and used to obtain data at higher irradiations. To ensure that several of the limited number of specimens a rig can carry were taken to a high dose, the programme of stored energy measurements had to be limited. To define the trend more precisely the thermal conductivity and total stored energy data were used; they were converted to $(\mathrm{d}E/\mathrm{d}T)_{400}$ values by using the empirical relations of figures 10 and 11. The derived values are quoted in tables 9 to 14. The increases of $(\mathrm{d}E/\mathrm{d}T)_{400}$ obtained from all reliable values at the five rig temperatures are shown in figures 12 to 16; it should be noted that data derived from other physical properties agree with the experimental $(\mathrm{d}E/\mathrm{d}T)_{400}$ data. The line drawn on each graph is *not* intended to be the best representation of those data; its significance is explained later.

It is of the utmost importance from the technical point of view to establish that the DIDO and Calder data are in agreement. Unless this can be done satisfactorily there will be considerable doubt that the high dose data from the material-testing reactors can be reliably assessed for power-producing reactors.

It has already been pointed out that there are two principal corrections, for equivalent dose and for equivalent temperature. The work described in §3 on dose calibration shows how the magnitudes of each have been separately established, in part by a simplified theory. There remains the direct experimental correlation of BEPO and Calder or of Calder and a material-testing reactor to avoid the doubtful theoretical step. This particular experiment is very difficult (it involves either a prolonged low-power operation in a material-testing reactor or the use of a refrigerated rig in Calder) and has not yet been undertaken. The direct comparison of rig and Calder data can only be used to check the combined effect of the two corrections.

PHILOSOPHICAL TRANSACTIONS OF THE ROYAL SOCIETY A MATHEMATICAL, PHYSICAL & ENGINEERING SCIENCES

The correspondence of Calder and rig data is examined by plotting Calder data on figures 12 to 16. The basis of correlation is that the $(\mathrm{d}E/\mathrm{d}T)_{400}$ values of specimens irradiated in Calder and in the rigs to the same equivalent dose at the same equivalent temperature should be the same. The equivalent temperatures of the Calder specimens cover the range

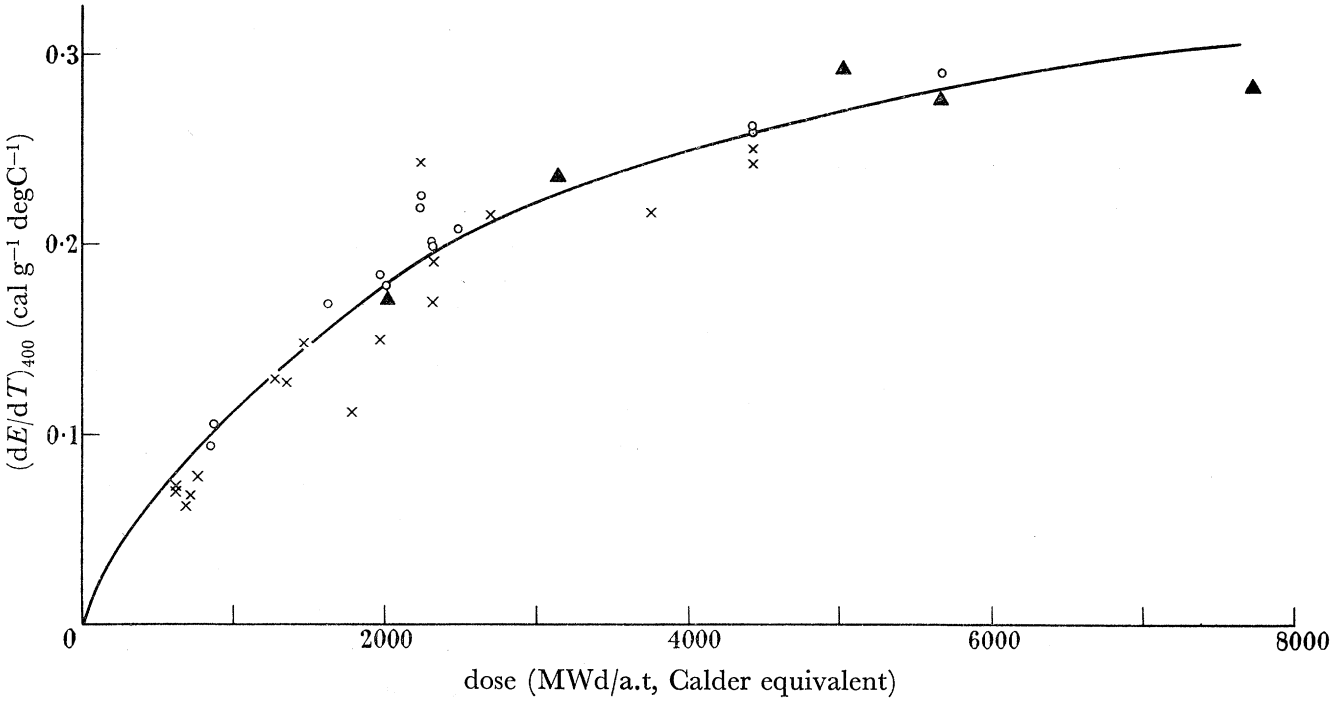

FIGURE 12. Variation of $(\mathrm{d}E/\mathrm{d}T)_{400}$ with dose for Calder equivalent temperature of 135 °C. ▲, Direct measurement of $\mathrm{d}E/\mathrm{d}T$; ○, from E; ×, from $K_0/K-1$; ———, scaled standard curve.

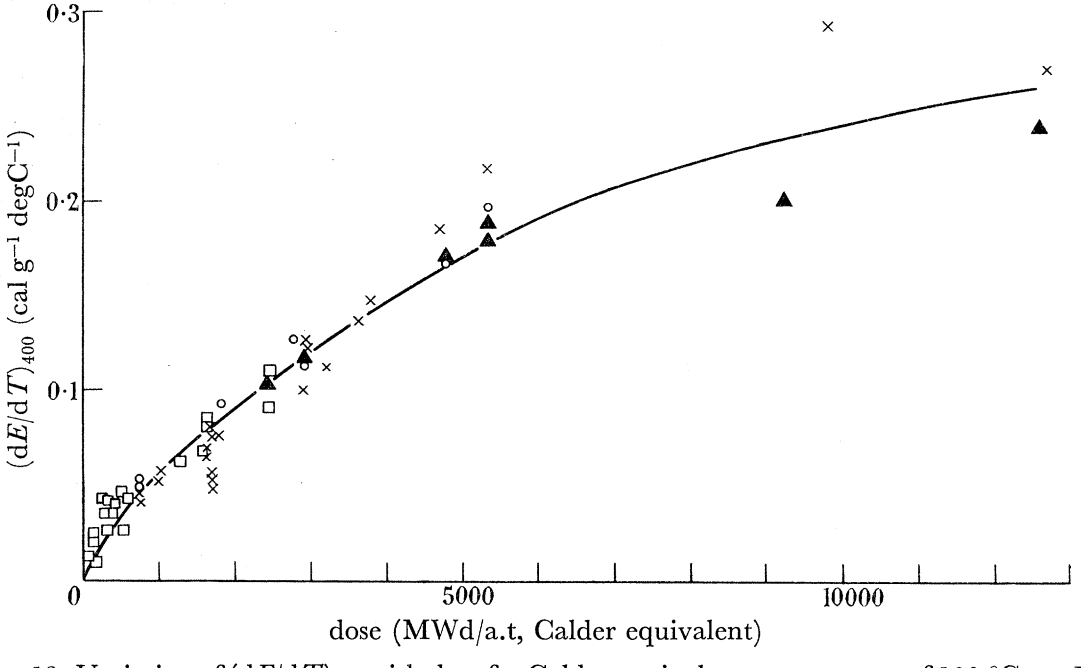

FIGURE 13. Variation of $(\mathrm{d}E/\mathrm{d}T)_{400}$ with dose for Calder equivalent temperature of 180 °C. ▲, Direct measurement of $\mathrm{d}E/\mathrm{d}T$; ○, from E; ×, from $K_0/K-1$; □, Calder data; ———, scaled standard curve.

PHILOSOPHICAL TRANSACTIONS OF THE ROYAL SOCIETY A MATHEMATICAL, PHYSICAL & ENGINEERING SCIENCES

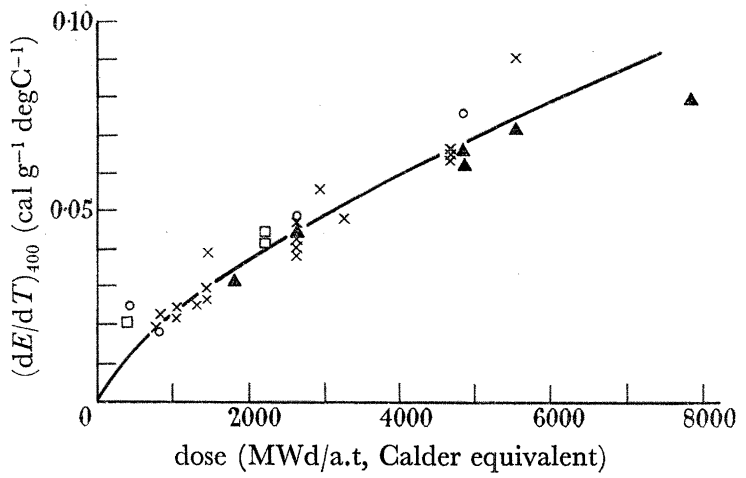

FIGURE 14. Variation of $(dE/dT)_{400}$ with dose for Calder equivalent temperature of 223 °C. ▲, Direct measurement of dE/dT; ○, from E; ×, from $K_0/K-1$; □, Calder data; ———, scaled standard curve.

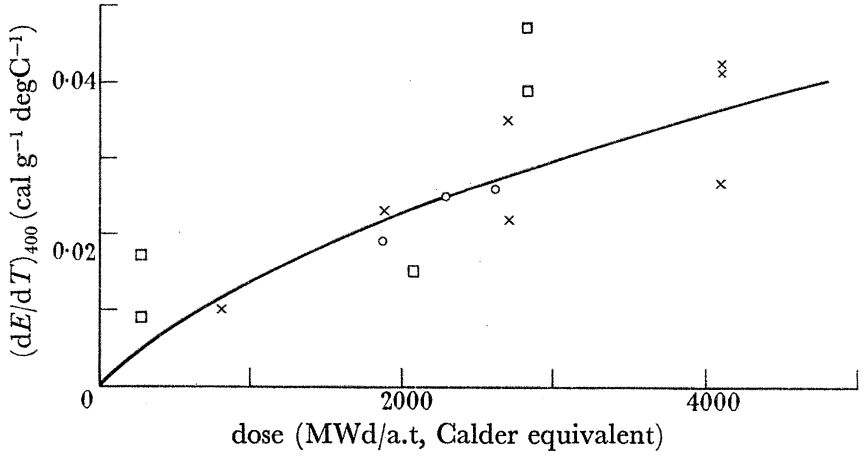

FIGURE 15. Variation of $(dE/dT)_{400}$ with dose for Calder equivalent temperature of 269 °C. ○, From E; ×, from $K_0/K-1$; □, Calder data; ———, scaled standard curve.

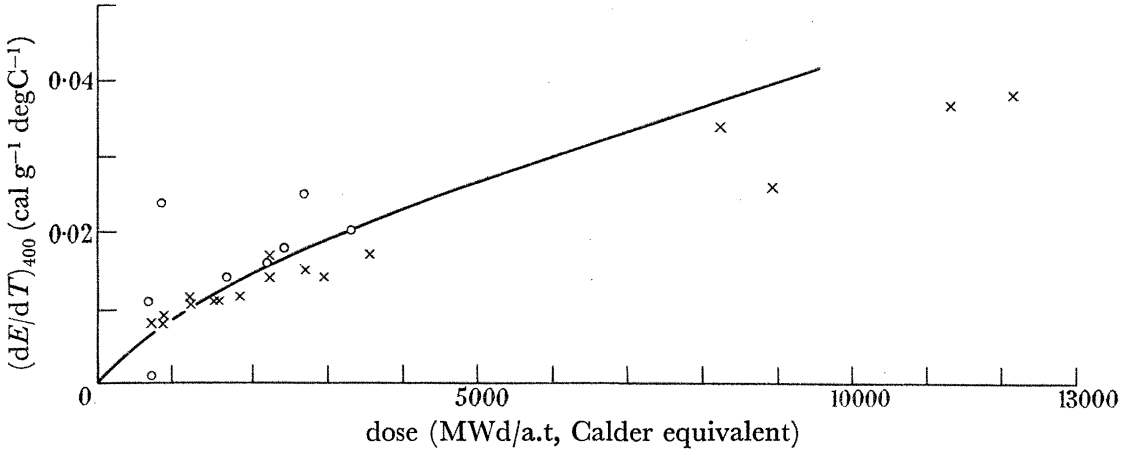

FIGURE 16. Variation of $(dE/dT)_{400}$ with dose for Calder equivalent temperature of 314 °C. ○, From E; ×, from $K_0/K-1$; ———, scaled standard curve.

155 to 338 °C, but in general there are no specimens with equivalent temperatures identical with those of the rigs. To obtain a reasonable number of points for comparison, all Calder data with an equivalent temperature within ±10 degC of the rig equivalent temperature are shown. About half the Calder points are direct observations of $(\mathrm{d}E/\mathrm{d}T)_{400}$ and the remainder from total stored energy. Inspection shows that the correlation of rig and Calder data is good. There is no doubt that the end-point of the calculations for correlation of dose and temperature is accurate within the limits of discrimination available with the present range of data. Although the comparison involves making two different corrections, its success gives good grounds for believing that the principles and separate quantitative values are reasonably accurate.

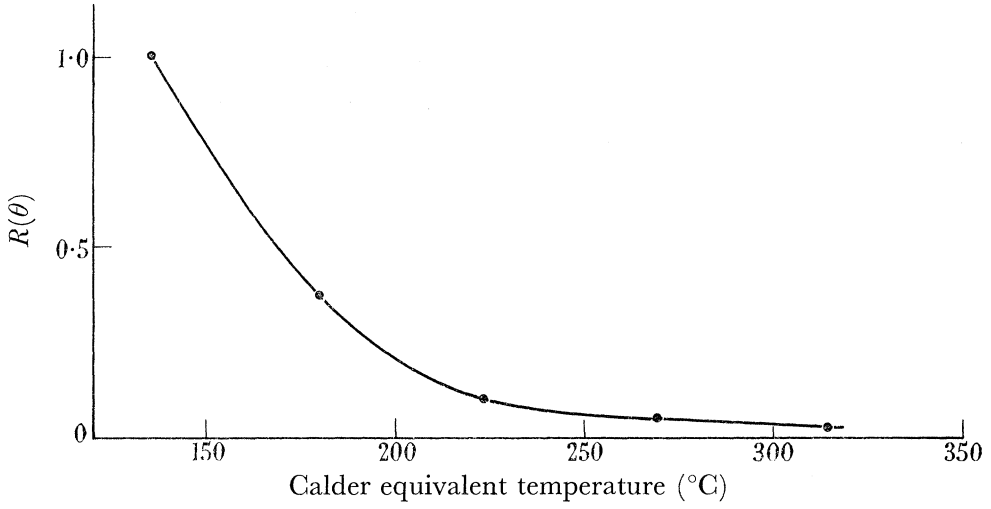

FIGURE 17. Factors correlating dose scales of figures 12 to 16 to make points fit a standard curve. Values of points are:

equivalent temperature (°C) ...	135	180	223	269	314
	1·000	0·370	0·100	0·048	0·025

The final task is to use the existing data to predict $(\mathrm{d}E/\mathrm{d}T)_{400}$ to levels approaching 0·3 cal g^{-1} $degC^{-1}$ or for doses up to 40000 MWd/a.t, whichever is reached first. It was assumed that all curves are of the same shape and can be related to each other by a change of scale on the dose axis. Since one of the curves goes as near 0·3 cal g^{-1} $degC^{-1}$ as is acceptable for design purposes, this assumption gives a well-defined solution.

The basic curve used is the one shown on figure 12, where the results from rig specimens irradiated at 150 °C are shown; it must be emphasized that this curve does not necessarily best fit the 150 °C data alone. The $R(\theta)$ values by which the doses on figure 12 have to be divided for the other equivalent temperatures are tabulated and shown graphically in figure 17. On figures 13 to 16 are shown curves calculated from that shown on figure 12 and the $R(\theta)$ values of figure 17.

An alternative method of showing the degree of success with which the common curve fits the data is demonstrated in figures 18 and 19. Figure 18 shows all the available rig data, and figure 19 all Calder data where the temperatures are reliable, fitted to the standard curve; the effective dose is the actual dose of the specimen multiplied by the appropriate $R(\theta)$ value.

Inspection of the way this method produces a curve which fits all data shows that it is reasonably successful in the early part of all curves, but that at the higher doses the $(dE/dT)_{400}$ values for the higher temperatures fall below the curve. There is a clear

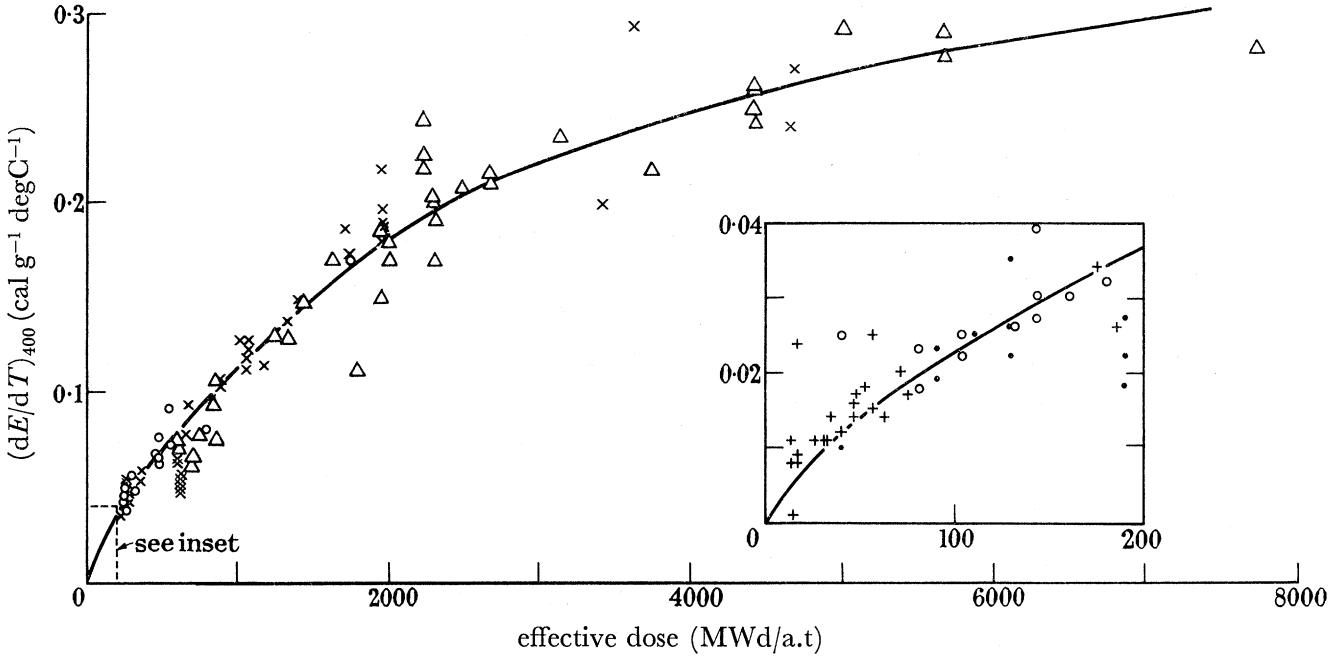

FIGURE 18. Rate of release of stored energy at 400 °C and effective dose $(R(\theta)\ D)$. Rig data. △, 150 °C rig; ×, 200 °C rig; ○, 250 °C rig; ●, 300 °C rig; +, 350 °C rig.

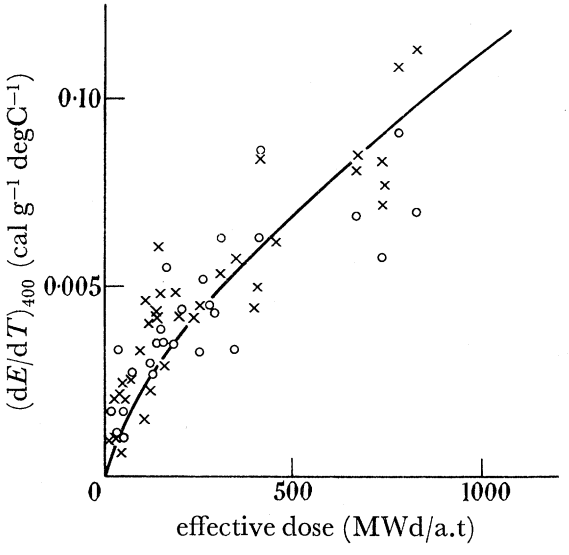

FIGURE 19. Rate of release of stored energy at 400 °C and effective dose $(R(\theta)\ D)$. Calder data. ×, Direct measurement of dE/dT; ○, from E.

impression of a tendency for $(dE/dT)_{400}$ to saturate at a level appreciably less than 0·3 cal g^{-1} $degC^{-1}$ at the higher irradiation temperatures. This is not unexpected, but since the results do not go far enough to demonstrate this experimentally and the effect cannot be predicted quantitatively, it cannot be taken into account without compromising the criteria for safety of design.

The basic curve of figure 18 and the $R(\theta)$ factors of figure 17 can now be used to calculate values of $(\mathrm{d}E/\mathrm{d}T)_{400}$ up to about 0·3 cal g^{-1} $degC^{-1}$ for all doses provided that Calder equivalent of the irradiation temperature lies between 135 and 314 °C. This is sufficient for all graphite-moderated reactors of the current type being built for electrical power generation since their temperatures lie within or above this range.

(*c*) *Discussion of reliability of assessment*

Some of the errors in this assessment can be expressed numerically; for instance, the experimental measurement of $(\mathrm{d}E/\mathrm{d}T)_{400}$ or the selection of the best value of the activation energy for equivalent temperature corrections. Others, for example the assumption that the basic shape of the curve is the same at all temperatures, cannot. There are three possible sources of error which require special consideration:

(*a*) The correlation of rig and Calder results by the equivalent dose and equivalent temperature concepts.

(*b*) The assumption of a common basic shape of curve at all temperatures.

(*c*) The use of $(\mathrm{d}E/\mathrm{d}T)_{400}$ as the relevant criterion for stored energy release.

Despite the fact that some of the individual data making up the correlation factor for rig and Calder results are not yet established as accurately as desirable, it has been demonstrated by direct comparison of the results that the net error is small. This agreement might be fortuitous in that self-compensating errors may be concealed. But since the current power-producing reactors are similar to Calder in geometry and rating, i.e. the individual data are combined in the same way, the use of the rig results for the design of those reactors will not lead to any serious error.

The second error certainly exists. The suggested method of interpretation shows rather larger values of $(\mathrm{d}E/\mathrm{d}T)_{400}$ arising at large doses at equivalent temperatures of 180 °C and upwards than will in fact arise. The error is therefore likely to produce a conservative design for the higher irradiation temperatures.

The third point cannot be resolved in detail without a full discussion of many features such as the detailed kinetics of stored energy release and of possible reactor incidents. The stored energy content of graphite is not a source of danger in a reactor, no matter what its level, provided that no departure from normal graphite operating temperatures occurs. Some rise in temperature caused by an accident, e.g. loss of coolant, is necessary before a significant release of stored energy begins. Stored energy becomes a hazard when it is sufficient for its release to contribute strongly to the course of an accident by causing the temperature to rise higher and more quickly, thus changing the consequences from something manageable to something not. Broadly the stored energy release is most important in the range between the irradiation temperature and the melting point of magnesium, 650 °C, since once magnesium fuel-element cans have melted other major sources of heat appear in the reactor. A second general reason why this range of temperature is important follows from the way the specific heat of unirradiated graphite increases with temperature (figure 8), since in many cases it is the difference between the specific heat and rate of stored energy release that is critical.

Thus the important point to decide is whether deductions from the variation of $(\mathrm{d}E/\mathrm{d}T)_{400}$ with dose and temperature lead to serious error in the range 200 to 650 °C.

Inspection of the curves available for dE/dT, of which examples are shown in figures 8 and 9, indicated that at low values of dE/dT, the curve decreases from a maximum some 125 °C above the irradiation temperature to a lower almost constant value above 500 °C. After higher doses, when the general level of the curve is higher, the value of dE/dT remains fairly constant to about 650 °C and thereafter rises, but no curve has been obtained for which $(dE/dT)_{600} > (dE/dT)_{400}$. Since the $(dE/dT)_{400}$ data have not been extrapolated beyond the measured range, the method employed here cannot underestimate $(dE/dT)_{600}$.

The data on which this work is based have been collected as the result of a joint programme covering many aspects of the U.K.A.E.A.'s field of endeavour. It is a pleasure to acknowledge the enthusiastic assistance of the sections and individuals concerned, in particular of H. G. Bullock and N. H. Hancock at AERE for work on rig development and operation; of A. Nicklin at Risley for heat-transfer calculations; of S. B. Wright of AERE for flux measurements; of Reactor Operations and Technical Staff at AERE, at Dounreay and at Calder Works, for assistance with the specimen irradiations; of the Risley Computer Section; of the Irradiation Physics Section at Windscale and of the Wigner Energy Group at AERE for undertaking the many detailed measurements.

The paper is published with the permission of Sir William Penney, F.R.S., Deputy Chairman, Sir William Cook, Member for Reactors, and Dr F. A. Vick, Director of Research Group of the United Kingdom Atomic Energy Authority.

References

Bell, J. C. & Greenough, G. B. 1957 *U.S./U.K. Graphite Conference.* Washington: United States Atomic Energy Commission. T.I.D.–7565 (part 1).

Command 471 1958 London: Her Majesty's Stationery Office.

Cottrell, A. H., Lomer, W. M., Simmons, J. H. W., Bell, J. C. & Greenough, G. B. 1958 *Second United Nations Conference on the Peaceful Uses of Atomic Energy.* A/Conf. 15/P/2485.

Davidson, D. F., Harrison, E. H., Mounsey, J. & Jacques, W. 1961 *U.K.A.E.A. T.R.G. Rep.* 53 (Ca).

Henson, R. W. & Mounsey, J. 1961 *U.K.A.E.A. D.E.G. Rep.* 328 (W).

Henson, R. W. & Simmons, J. H. W. 1959 *U.K.A.E.A. Rep.* AERE M/R 2564.

Jackson, G. F. & Cordall, D. 1959 *U.K.A.E.A. Rep.* IGR. 189 (RD/W).

Lomer, W. M. 1957 *U.S./U.K. Graphite Conference.* Washington: United States Atomic Energy Commission, T.I.D.–7565 (part 1).

Moore, R. V. & Goodlet, B. L. 1957 *J. Brit. Nuclear Energy Conf.* (2) **2**, 48–54.

Nightingale, R. E. 1957 *U.S./U.K. Graphite Conference.* Washington: United States Atomic Energy Commission TID–7565 (part 1).

Nightingale, R. E., Davidson, J. M. & Snyder, W. A. 1958 *Second United Nations Conference on the Peaceful Uses of Atomic Energy.* A/Conf. 15/P/614.

Nightingale, R. E. & Fletcher, J. F. 1957 *U.S.A.E.C. Res. Develop. Rep.* H.W.–47776 REV.

O'Driscoll, W. G. & Bell, J. C. 1960 *Materials for nuclear engineering*, chap. 7. Graphite. London: Temple Press Books.

Simmons, J. H. W. 1960 *Progress in nuclear engineering*, series IV, vol. 3, pp. 327–347. London Pergamon Press.

Woods, W. K., Bupp, L. P. & Fletcher, J. F. 1956 *Proceedings of the International Conference on the Peaceful Uses of Atomic Energy.* VMIA/CONF 8/P/746.

PHILOSOPHICAL TRANSACTIONS OF THE ROYAL SOCIETY A MATHEMATICAL, PHYSICAL & ENGINEERING SCIENCES